N O T I C E

THIS DOCUMENT HAS BEEN REPRODUCED FROM
MICROFICHE. ALTHOUGH IT IS RECOGNIZED THAT
CERTAIN PORTIONS ARE ILLEGIBLE, IT IS BEING RELEASED
IN THE INTEREST OF MAKING AVAILABLE AS MUCH
INFORMATION AS POSSIBLE

Department of Mechanical

and Aerospace Engineering

Effect of a Finite Ionization Rate on the Radiative Heating of Outer Planet Atmospheric Entry Probes

BY

H. F. Nelson

August 1981

University of Missouri-Rolla

NASA

Technical Memorandum 82094

DIRECTIONALITY EFFECTS IN THE TRANSFER OF X-RAYS FROM A MAGNETIZED ATMOSPHERE: BEAM PULSE SHAPES

P. Mészáros and S. Bonazzola

FEBRUARY 1981

Effect of a Finite Ionization Rate on the Radiative
Heating of Outer Planet Atmospheric Entry Probes

by

H. F. Nelson

Thermal Radiative Transfer Group
Department of Mechanical and Aerospace Engineering
University of Missouri-Rolla
Rolla, Missouri   65401
August 1981

CONTENTS

FIGURES

TABLES

ABSTRACT

The influence of finite rate ionization in the inviscid gas just behind the stagnation shock wave on the radiative heating of probes entering the hydrogen-helium atmosphere of the major planets has been investigated. At the present time, there is disagreement as to whether the radiative flux increases or decreases relative to its equilibrium value when finite rate ionization is considered. Leibowitz and Kuo contend that the finite rate ionization in the hydrogen gas just behind the shock wave reduces the radiative flux to the probe, whereas Tiwari and Szema predict that it increases the radiative flux. The radiation modeling used in the calculations of both pairs of these investigators has been reviewed. Tiwari and Szema assumed a Boltzmann population at the local electron temperature for the electronic states of hydrogen. The electron temperature just behind the shock is higher than the temperature for equilibrium flow field calculations. This increases the radiative source function and the excited state populations, both of which increase the radiative emission in the Balmer region of the spectrum. Because shock layers are optically thin in this spectral region, the increased emission directly increases the radiative heat transfer to the probe. The finite rate ionization model developed by Leibowitz involves the assumption that the excited state population is in equilibrium with the electrons at the electron temperature. It also involves a finite excitation rate. This model predicts low excited state populations just behind the shock as compared to equilibrium chemistry solutions. The lower excited state populations reduce the radiative emission just behind the shock and in turn decrease the radiative heating to values less than those predicted by equilibrium chemistry solutions. It is concluded that finite rate ionization in the inviscid region of the shock layer should reduce the cold wall radiative heating below the values predicted by equilibrium chemistry assumptions.

4

INTRODUCTION

Radiation forms a significant fraction of the heat transferred to a probe that enters the atmosphere of Jupiter or Saturn. In reality, the design of the heat shield for such a probe is controlled by the radiation heat transfer. At present, the United States does not have experimental facilities capable of producing the extreme thermodynamic conditions necessary to test the heat shield designs for Jupiter or Saturn entry. Thus, the heat shields must be designed based upon analytical models of the flow field and heat transfer phenomena. The theoretical and numerical models must be as accurate as possible. In order to improve the heat transfer predictions, Leibowitz and Kuo[1,2] and Tiwari and Szema[3,4] investigated the influence of finite rate ionization in the inviscid part of the stagnation shock layer on radiative heating of probes during Jupiter and Saturn atmospheric entry. Both investigative teams considered cold wall inviscid models for the probe shock layer. However, they reached opposite conclusions as to how the ionization rate assumption affects the radiative transfer. Tiwari and Szema[3,4] contended that the radiation heating at the probe stagnation point increased, whereas Leibowitz and Kuo[1,2] predicted that it decreased relative to the results obtained when the ionization rate was assumed to be in equilibrium at the local thermodynamic conditions.

Present State of Knowledge

The first studies of finite ionization rate effects on the radiative heating of probes entering the atmospheres of Jupiter, Saturn, and Uranius were presented by Leibowitz and Kuo[1,2] and Howe[5]. These studies indicated that the assumption of a finite ionization rate predicts significant reductions in the radiative heating as compared to equilibrium ionization predictions. Leibowitz and Kuo[2] found that a nonequilibrium ionization layer with reduced radiative

emission exists just behind the stagnation point shock wave during part of the entry into model atmospheres of Jupiter and Saturn. They predicted that the radiative heating rate, calculated using the finite ionization rate assumption, could be up to 40% lower than if the heating rate were calculated by assuming that the plasma ionization takes place in equilibrium. However, the reduction in total probe heating, which was calculated by integrating both the radiative and convective heating rates over the atmospheric entry time, was less than 15%. The low reduction in total heat transfer occurred, because, when the finite ionization rate radiative fluxes were very low (compared to the equilibrium ionization rate radiative fluxes), the heating was largely due to convection.

Leibowitz and Kuo[2] calculated the radiative flux to the probe for both the equilibrium and finite ionization rate assumptions by using the results of the hydrogen-helium radiation computations of Stickford[6]. They computed the instantaneous values for the radiative flux at the thermodynamic conditions obtained from both the finite and equilibrium ionization rate assumptions at each point along the trajectory and integrated the results to obtain the total radiative heating.

Tiwari and Szema[3,4] also considered the effect of finite ionization rates on the radiative heating of probes entering the Jovian atmosphere. Their results showed that the assumption of a finite ionization rate increased the radiative heating rate by about 10% as compared to the heating rate obtained by assuming equilibrium ionization. They used a fundamental fluid mechanics model and the same ionization rate constants that Leibowitz and Kuo[1,2] used; however, they employed a detailed 58-step, spectral, absorption coefficient model for the hydrogen-helium plasma to calculate the radiation transport.

Zoby and Moss[7] conducted a preliminary investigation of the thermal environment and heating rates for a probe entering the atmosphere of Saturn. They

used the numerical code developed by Tiwari and Szema to determine the effect of a finite ionization rate in the inviscid part of the stagnation shock layer on the heat transfer to the probe. Their results indicate that the assumption of a finite ionization rate would significantly increase the radiative heat transfer rate at the probe stagnation point as compared to equilibrium ionization and that the finite ionization rate effects on radiative heating would become negligible away from the stagnation point. However, they did not allow the electrons and atoms to have different temperatures.

These previous investigations show that the assumption of a finite ionization rate influences the radiative transfer and, hence, the design of the heat shields of probes intended for atmospheric entry of major planets. The nonequilibrium ionization layer just behind the shock wave influences the radiation transfer at or near the stagnation point. However, the radiative heating for the assumption of a finite ionization rate has been shown either to increase or decrease relative to its value for equilibrium ionization for roughly the same physical conditions in two independent investigations. This contradiction is investigated in the present study.

The present study is limited to an investigation of the underlying reasons for the opposite conclusions reached in the work of Leibowitz and Kuo[1,2] and Tiwari and Szema[3,4] for nonviscous, hydrogen-helium shock waves with a cold nonblowing wall boundary condition at the probe heat shield. The effects of ablation and the ablation layer gases are not considered. The study is limited to the stagnation shock layer. Appendix A contains a survey of the present state of knowledge of nonequilibrium shock wave structure.

SHOCK WAVE STRUCTURE

This section contains a short introduction to nonequilibrium shock wave structure. A detailed review is included in Appendix A. Figure 1 shows the shock wave structure for a typical atomic gas taken from reference 8. The figure is for a Mach 24 shock wave in argon; however, it is similar to that of a hydrogen-helium shock wave, because the hydrogen dissociates almost instantly behind the shock. The pressure in front of the argon shock is 1 cm Hg, and the temperature is 300 K. The parameters shown are all nondimensional with temperatures, $\bar{T}_i = T_i/(16,800 \text{ K})$, $i = a$, e, and density $\bar{\rho} = \rho/(.000229 \text{ gm/cm}^3)$. The reference value of the degree of ionization is $\alpha_0 = 0.449$. The parameter τ_g represents the ground state continuum optical thickness. The reference values of temperature, density, and α_0 are the equilibrium values behind the shock wave. Note that the nondimensional parameters representing these variables all go to unity as the gas goes to equilibrium. The nondimensional atom-atom and electron-atom ionization rates are given by $\dot{n}_{AA}/n_s$ and $\dot{n}_{eA}/\dot{n}_s$, respectively.

The gas behind the shock wave is in thermal nonequilibrium, with the heavy particles much hotter than the electrons $(\bar{T}_a > \bar{T}_e)$. As one moves into the relaxation region behind the viscous shock, $\bar{T}_e$ rapidly increases to about its equilibrium value and then slowly increases until it becomes equal to $\bar{T}_a$ and thermal equilibrium occurs.

Initially, just behind the shock wave, the degree of ionization is increased by atom-atom collisions. When the electron population is sufficiently high, electron-atom collisions become the major producers of electrons. Each electron produced via an electron-atom collision requires that the electron gas as a whole supply the necessary ionization energy. Thus, the electron gas is cooled by ionizing collisions with the atom gas. At the same time, the electron gas receives energy by elastic collisions with the atom gas and thereby reduces $\bar{T}_a$.
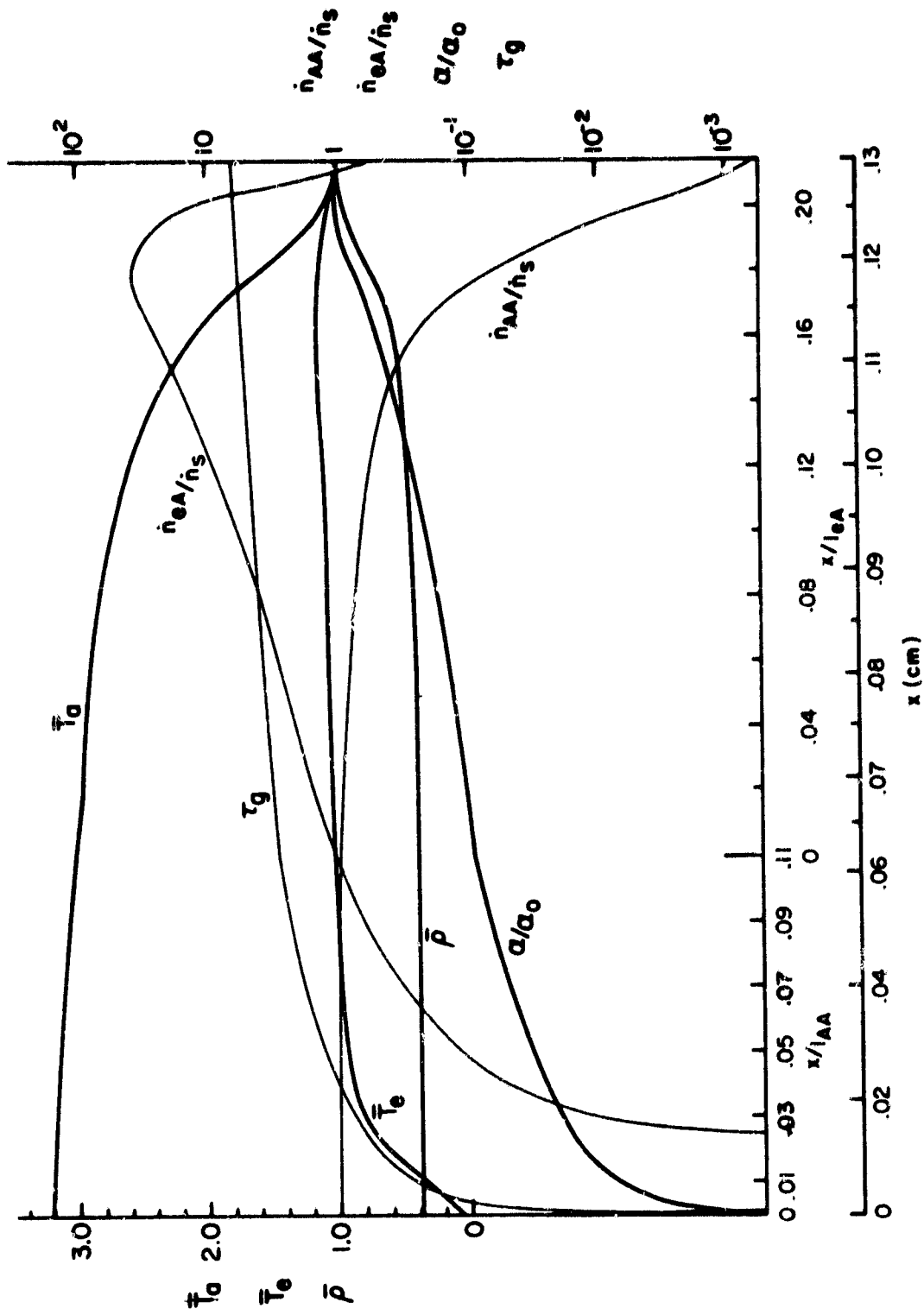
Figure 1. P = 1 cm Hg, Trapped Radiation, Mach 24 Shock Wave in Argon: $\rho_0 = 2.285 \times 10^{-4}$ gm/cm^3, $T_0 = 16,828$ K, and $\alpha_0 = 0.449$.

9

Throughout most of the relaxation region, the energy gained by the electron gas through elastic collisions with the atom gas is almost balanced by the loss of energy through electron-atom ionizing collisions. This keeps the electron temperature roughly constant throughout most of the relaxation region.

The argon atom was modeled as if it had only two electronic states: a ground state and an excited state as shown schematically in Figure 2. The single excited state of the model represents all the excited states of the atom. Thus, the radiation model involves only one bound-bound process and two bound-free processes. This type of two-state model has been widely used in numerical shock wave structure studies. It generally predicts results that agree well with experiment.

Figure 1 shows that the ground-state continuum optical thickness, τ_g, has a value of about 8 at the end of the relaxation region. This implies that the ground-state continuum radiation emitted near the shock wave will not penetrate to the end of the relaxation region, because most of the radiation energy absorbed within two optical path lengths of its emission point. The excited state continuum optical thickness is too small to be shown on Figure 1. Thus, excited state continuum radiation emitted just behind the shock can easily penetrate to the end of the relaxation region. However, the excited state source function is very weak just behind the shock, because there are not very many free electrons available to recombine to an excited atomic state, and in the process emit radiation.

10
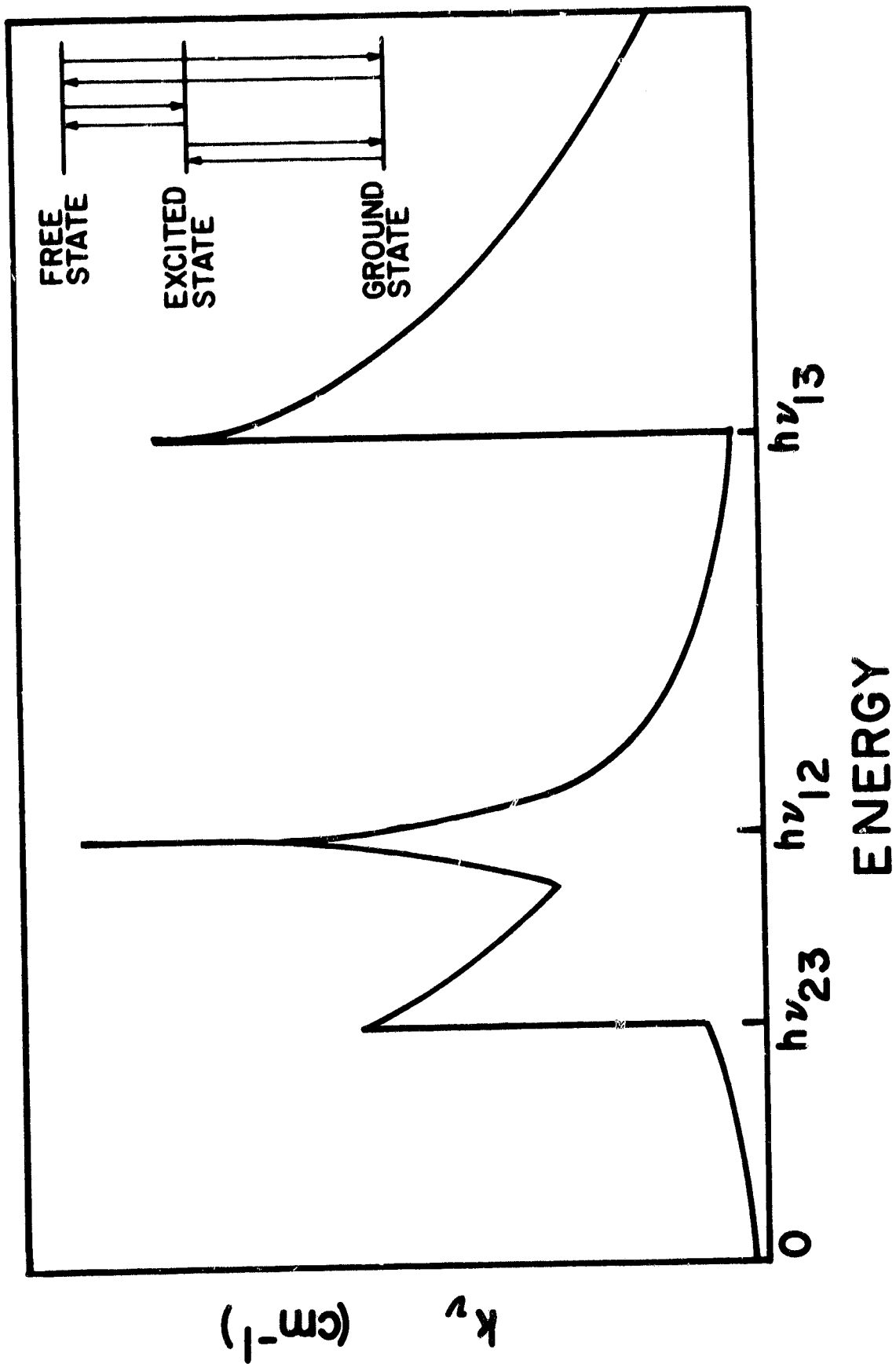
Figure 2. Schematic of the Radiation Absorption Coefficient for a Two-Level Atomic Gas.

11

Collision Processes

Leibowitz[1] developed a reaction scheme describing the important collisional processes in hydrogen-helium ionizing shock waves that were modeled after results obtained from studies of argon ionization. Reactions are included for dissociation of molecular hydrogen, excitation of the electronic states of atomic hydrogen and helium, and ionization of the hydrogen and helium by collisions with atoms and electrons. The reaction scheme and rate constants are listed in Table 1.

In the reaction scheme, the atomic hydrogen and helium are assumed to have two bound states: a ground state and a first excited state as shown schematically in Figure 2. The first excited state is a representative state, which represents all the excited states. The two-state assumption is a good model when the ground and first excited states are separated by a large energy gap as compared to the energy difference between the first excited state and the ionization energy. For these types of gases, the excited states and electrons have nearly the same energy. Thus, it is also assumed that the excited state and electron populations are in equilibrium with each other at the electron temperature.

The dissociation rate for molecular hydrogen was obtained from shock tube investigations[1]. Hydrogen initially dissociates by collisions with itself and helium and, subsequently, by collisions with atomic hydrogen, ions, and electrons. For the thermodynamic conditions of interest in outer planet atmospheric entry, dissociation is completed before ionization begins, so that the dissociation and ionization processes are uncoupled.

The ionization of atomic hydrogen is initiated by atom-atom collisions, which produce atoms with electronically excited states. The excited atoms are ionized by additional collisions. The reaction scheme assumes that hydrogen

Table 1	Reaction scheme and rate constants for hydrogen-helium chemical nonequilibrium conditions. (From Leibowitz, Ref. 1)

Reactions	Rate constants in cm^3 sec^{-1} $mole^{-1}$
1. $H + e \rightleftarrows H^+ + 2e$	$k_1 = 2.27E13 \; T_e^{1/2} \exp(-157,780/T_e)$
2. $He + e \rightleftarrows He^+ + 2e$	$k_2 = 1.33E13 \; T_e^{1/2} \exp(285,160/T_e)$
3. $H + e \rightleftarrows H^* + e$	$k_3 = 4.11E13 \; T_e^{1/2} \exp(-116,010/T_e)$
4. $He + e \rightleftarrows He^* + e$	$k_4 = 2.24E13 \; T_e^{1/2} \exp(-232,030/T_e)$
5. $H + H \rightleftarrows H^* + H$	$k_5 = 6.20E10 \; T^{1/2} \exp(-116,010/T)$
6. $H + He \rightleftarrows H^* + He$	$k_6 = 4.89E10 \; T^{1/2} \exp(-116,010/T)$
7.[a] $H_2 + He \rightleftarrows H + H + He$	$k_7 = 4.33E18 \; T^{-1} \; [1 - \exp(-15E8/T^2)]$ $\exp(-52340/T)$
8. $H_2 + H_2 \rightleftarrows H + H + H_2$	$k_8 = 2.5 \; k_7$
9.[a] $H_2 + H \rightleftarrows H + H + H$	$k_9 = 14.0 \; k_7$
10. $H_2 + H^+ \rightleftarrows H + H + H^+$	$k_{10} = k_9$
11. $H_2 + e \rightleftarrows H + H + e$	$k_{11} = k_9$

All temperatures are °K.

[a] Reaction rates k_7 and k_9 modified from the expressions of Leibowitz[1] by Tiwari and Szema[3,4].

in the first excited state is produced by collisions with hydrogen (reaction 5) and helium (reaction 6). Excitation to the first excited state is the rate limiting step for ionization. The excited atoms are rapidly ionized by further collisions.

As the result of atom-atom collisions, the population of free electrons increases as one moves deeper into the shock layer. When the number of electrons reaches a certain magnitude, the electron-atom collisions become more important than the atom-atom collisions. Electron-atom collisions produce hydrogen ions by the same type of two-step process as the atom-atom collisions do. The electron is first excited by reactions 3 and 4 and then it is ionized.

In summary, the reaction scheme developed by Leibowitz involves a two-step ionization process in which the excitation to the first excited state is the rate controlling reaction. In other words, the rate of excitation is finite in the model and the first excited state is not populated to its Boltzmann value. Thus, the Leibowitz model really allows for both nonequilibrium excited state and electron populations. The finite rate ionization model also includes the assumption that the excited state population is in equilibrium with the electron population at the electron temperature[9]. Consequently, the model predicts low excited state populations just behind the shock wave, as compared to equilibrium chemistry solutions.

Radiation Processes

The general equations for the radiation absorption coefficient and source function are developed for a nonequilibrium atomic gas in Appendix B. The radiation absorption coefficient as given by Eq. 36, Appendix B, can be rewritten for a two-level atom as follows:

$$k_\nu = n_a(1)\sigma_{1f}[1 - Z_{1f}\exp(-h\nu/kT_e)] + n_a(2)\sigma_{2f}[1 - Z_{2f}\exp(-h\nu/kT_e)]$$

$$+ n_a(1)\sigma_{12}[1 - Z_{12}\exp(-h\nu/kT_a) \tag{1}$$

14

The source function for a two-level atom from Eq. 39, Appendix B, becomes

$$S = \frac{2h\nu^3}{c^2} \left[\frac{(n_a(1)\sigma_{1f}Z_{1f} + n_a(2)\sigma_{2f}Z_{2f})\exp(-h\nu/kT_e) + n_a(1)\sigma_{12}Z_{12}\exp(-h\nu/kT_a)}{k_\nu} \right] \quad (2)$$

where T_e represents the electron temperature and T_a the atom temperature.

The expression for S_ν and k_ν as written above are for energies $h\nu$ greater than the ground state ionization edge. For energies ($h\nu$) less than the ground state ionization edge, σ_{1f} is zero. Likewise, for energies ($h\nu$) less than the excited state ionization edge, both σ_{1f} and σ_{2f} are zero. Also, σ_{12} is a function of frequency, because it includes the line shape.

For the assumption that the excited states and electrons are in equilibrium at the electron temperature, one can write the expressions for Z_{12}, Z_{1f}, and Z_{2f} in terms of T_e and T_a. The expression for Z_{12} becomes

$$Z_{12} = \frac{n_a(2)}{n_a(1)} \left[\frac{n_a^*(1)}{n_a^*(2)} \right]_{T_a} = \frac{n_a(2)}{n_a(1)} \frac{g_1}{g_2} \exp(\chi_{12}/kT_a), \quad (3)$$

where χ_{12} is the energy difference between the ground and excited state and where the bound electronic states are in equilibrium at the atom temperature when the atom is in equilibrium. Since the excited state $n_a(2)$ is assumed to be in equilibrium with the electrons at T_e, one can relate $n_a(2)$ to n_e by

$$\frac{n_e^2}{n_a(2)} = 2 \frac{(2\pi m_e kT_e)^{3/2}}{h^3} \frac{g_i}{g_2} \exp(-\chi_2/kT_e), \quad (4)$$

where χ_2 is the ionization energy for the excited state. If $n_a(1)$ is in equilibrium with the electrons at the electron temperature, one has

15

$$\frac{n_e^2}{n_a^*(1)_{T_e}} = \frac{2(2\pi m_e kT_e)^{3/2}}{h^3} \frac{g_1}{g_1} \exp(-\chi_1/kT_e),$$ (5)

where χ_1 is the ground state ionization energy. Eliminating n_e from Eqs. (4) and (5), one can relate $n_a(2)$ to $n_a^*(1)_{T_e}$ and write

$$\frac{n_a(2)}{n_a(1)} \approx \frac{n_a^*(1)_{T_e}}{n_a(1)} \frac{g_2}{g_1} \exp(-\chi_{12}/kT_e).$$ (6)

Thus, Z_{12} can be written as

$$Z_{12} = \frac{n_a^*(1)_{T_e}}{n_a(1)} \exp\left[\frac{-\chi_{12}(T_a - T_e)}{kT_a T_e}\right],$$ (7)

where $n_a^*(1)_{T_e}$ is given in terms of n_e and T_e by Eq. (5). Note that as the gas approaches equilibrium Z_{12} approaches unity.

One can write Z_{1f} as

$$Z_{1f} = \frac{n_e^2}{n_a(1)} \cdot \left[\frac{n_a^*(1)}{n_e^{*2}}\right]_{T_e} = \frac{n_e^2}{n_a(1)} \frac{g_1}{g_1} \frac{h^3 \exp(\chi_1/kT_e)}{2(2\pi m_e kT_e)^{3/2}}$$ (8)

where the free states and the bound states are in equilibrium at the electron temperature when the gas is in equilibrium. If one eliminates n_e by using Eq. (5), he obtains

$$Z_{1f} = \frac{n_a^*(1)_{T_e}}{n_a(1)}$$ (9)

where $n^*(1)_{T_e}$ is defined in terms of the local electron number density and the electron temperature by Eq. (5). Note that Z_{1f} approaches unity as the gas goes to equilibrium.

The parameter Z_{2f} is always unity, because the excited states and electrons are in equilibrium at the electron temperature.

As a consequence of Eqs. (3) through (9), one can rewrite Eq. (1) for the absorption coefficient as

$$k_\nu = n_a(1)\sigma_{1f}\{1 - \frac{n_a^*(1)_{T_e}}{n_a(1)} \exp(-h\nu/kT_e)\} + n_a(2)\sigma_{2f}\{1 - \exp(-h\nu/kT_e)\}$$

$$+ n_a(1)\sigma_{12}\{1 - \frac{n_a^*(1)_{T_e}}{n_a(1)} \exp[\frac{-\chi_{12}(T_a - T_e)}{kT_a T_e}] \exp(-h\nu/kT_a)\}. \tag{10}$$

Equation (2) for the source function becomes

$$S_\nu = \frac{2h\nu^3}{c^2}\left[\frac{[n_a^*(1)_{T_e}\sigma_{1f} + n_a(2)\sigma_{2f}] \exp(-h\nu/kT_e)}{k_\nu}\right.$$

$$\left.+ \frac{n_a^*(1)_{T_e}\sigma_{12} \exp[-\chi_{12}(T_a - T_e)/(kT_a T_e)] \exp(-h\nu/kT_a)}{k_\nu}\right]. \tag{11}$$

As noted above, one must be careful in the application of these equations because of the spectral behavior of σ_{1f} and σ_{2f}. Note that as the gas approaches equilibrium, S_ν becomes the Planck function, and the absorption coefficient becomes the product of the stimulated emission factor $(1 - \exp(-h\nu/kT))$ and a term dependent upon the number densities of the bound states. The bound state population becomes Boltzmann distributed at equilibrium.

Equations (10) and (11) show that the radiation source function and absorption coefficient differ from their equilibrium values for the H_2-He ionization model. Tiwari and Szema[3,4] used equilibrium values for the source function and absorption coefficient. They evaluated k_ν and S_ν at the electron temperature. As discussed below, this assumption for k_ν and S_ν leads to increased radiative heating for the outer planet atmospheric entries as compared to a total equilibrium solution.

FINITE RATE IONIZATION

The finite rate ionization model for hydrogen-helium gas mixtures has been used in investigations of the radiative heating of vehicles entering the atmosphere of Jupiter and Saturn. Table 2 lists a few of these investigations and contains the ambient conditions, the probe nose radii, the shock wave stand-off distances, and the radiation fluxes at specific points in the entry trajectories for three cases. The solutions shown in Table 2 are for roughly the same entry conditions. Table 2 gives the comparison of the radiative flux for an equilibrium solution and a finite ionization rate solution attained from the same numerical code. The solutions obtained with the Leibowitz code[2] show that finite rate ionization produces a decrease in the radiative heating rate, whereas those obtained with the Tiwari and Szema[3,4,7] code show that it produces an increase in the radiative heating rate relative to equilibrium ionization solutions. Note that in one of the cases, the equilibrium solution of Moss[10] was used as a comparison case.

The solutions of Moss[10] were obtained from an equilibrium viscous shock layer numerical code, which includes a detailed description of the radiative transport, equilibrium chemistry, and transport properties. The analysis allowed for ablation injection at the heat shield and either laminar or turbulent flow. The set of equations describing the flow were obtained from the steady-state Navier-Stokes equations by retaining terms up to second order in the inverse square root of the Reynolds number. This numerical code was used to produce "benchmark" solutions for the design of the Galileo Probe heat shield.

Tiwari and Szema[3,4] developed a viscous shock layer numerical code similar to that of Moss[10] to solve the steady-state shock layer equations. Their analysis is restricted to nonblowing laminar flow fields about hyperboloid bodies. Equilibrium and finite rate chemistry and thermal equilibrium or non-equilibrium

Table 2.   Predictions of Equilibrium and Finite Rate Radiative Fluxes

	Conditions at infinity in front of shock			Probe Nose Radius	Shock Stand-off distance	radiation flux	
	V_∞ km/sec	T_∞ °K	ρ_∞ Kg/m³	R cm	δ cm	q_{eq} Mw/m²	q_{non-eq} Mw/m²
Saturn Traj II [7,10] T = 51.75 sec atm = 89/11	29.3	83.9	.000579	31.1	2.54	40.0[a]	71.7[b]
Saturn Entry [3] Z = 115 Km atm = 85/15	39.1	145.0	.000465	23	2.02	422.6[c]	464.3[c]
Saturn Entry [2] T = 18 sec atm = 73/27	15 degree entry			25		37.0[d]	20.0[d]

a. Moss, reference 10

b. $T_e = T_a$ for non-equilibrium solution. Zoby and Moss, ref. 7 (using Tiwari and Szema Code, ref. 3)

c. Tiwari and Szema, ref. 4, pp. 161

d. Leibowitz and Kuo, ref. 2, Fig. 7

options are included in the code. The equilibrium chemistry uses an approximate equation of state. The finite rate chemistry uses the rate constants and ionization model of Leibowitz[1]. A 58-step spectral model for the absorption coefficient of the hydrogen-helium gas mixture was used to calculate the radiation transport.

Leibowitz and Kuo[2] developed a simplified rapid numerical method to calculate a first order approximate solution for the flow field. They used correlations for the shock wave shape and stand-off distance and solved for the flow along stream tubes. Many details were omitted. The radiation calculations were uncoupled from the flow field calculations; however, they were correlated to the local thermodynamic state of the gas. A reaction similarity parameter, Ω, which represents the ratio of the fluid mechanic residence time to reaction time, was used to correlate the electron distribution in the shock layer. When Ω was small ($\sim$ 1), the ionization rate was finite. When Ω was large ($\sim$ 20), the ionization was in equilibrium.

Leibowitz and Kuo Solution

Figure 3 shows a shock layer solution obtained by Leibowitz and Kuo[2] for the electron temperature and the electron concentration for two values of Ω at a shock layer position slightly displaced from the stagnation point. For the equilibrium solution, the electron temperature is approximately constant across the shock layer. In the finite rate case, T_e is high just behind the shock and decreases to its equilibrium value near the body. For equilibrium flow, the electron concentration is roughly constant across the shock layer, and for finite rate ionization, it is very low near the shock and increases to its equilibrium flow value near the body. In the Leibowitz finite rate ionization model, the excited state population is related to the electron concentration. In other words, it would be small just behind the shock and increase to its equilibrium value near the body just as the electron concentration does.
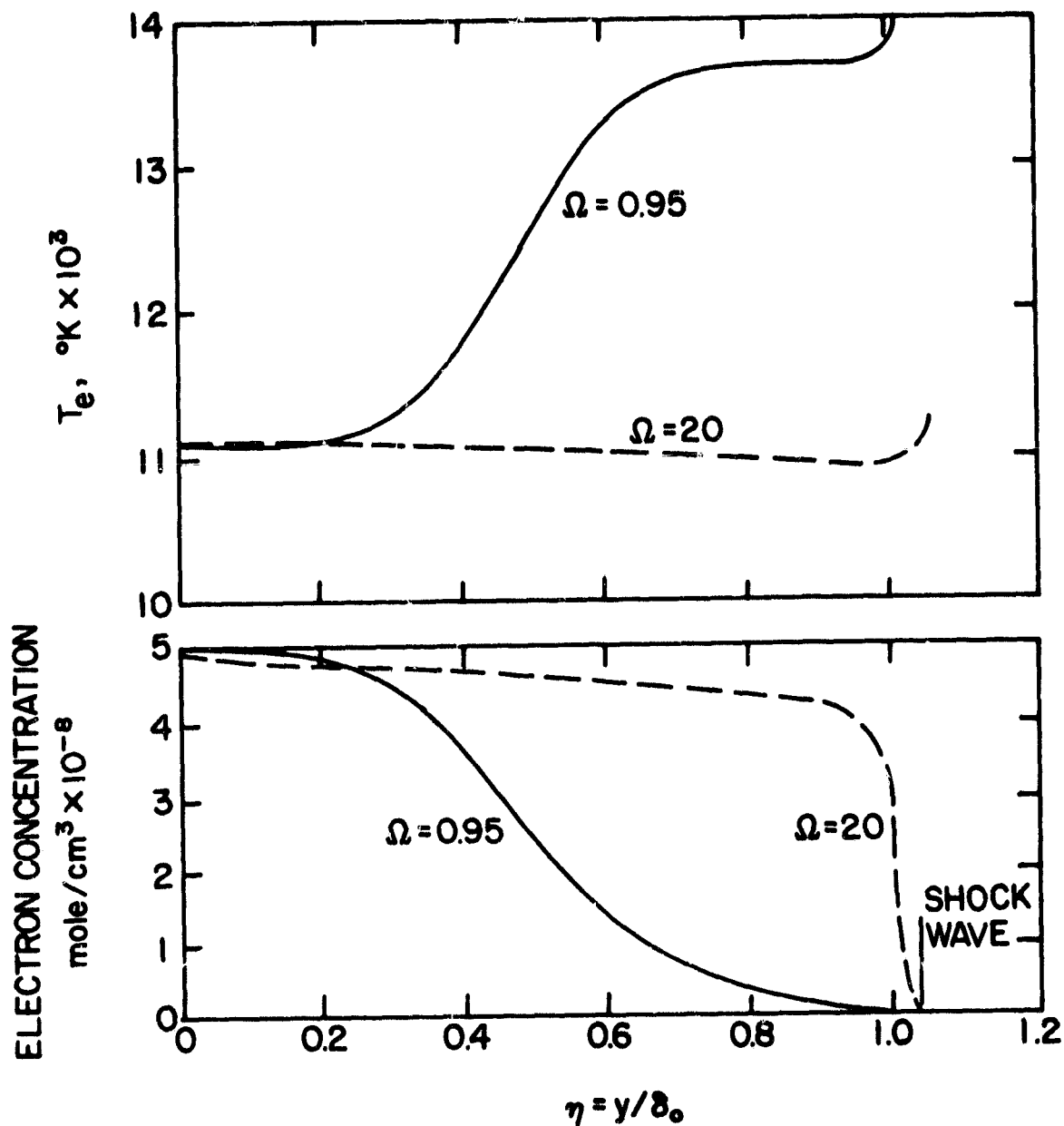
Figure 3. Electron Temperature and Electron Concentration as a Function
of Nondimensional Position across the Shock Layer. $\Omega = 20$
represents Equilibrium Flow, $\Omega = 0.95$ represents Nonequilibrium
Flow, $\delta_0 = 1.7$ cm. The Data is for $\theta = 0.20$ Radians, where
$\theta = 0$ at the Stagnation Point. (From Ref. 2)

Tiwari and Szema Solution

Tiwari and Szema[3,4] used a detailed numerical analysis to calculate the flow field and to predict the radiation heating of outer planet atmospheric entry vehicles. They calculated the shock layer composition by using the finite rate ionization model developed by Leibowitz. Figures 4 and 5 show a typical solution for the electron and atom temperature and the composition at the stagnation point for both equilibrium ionization and finite ionization rate flow. The solution has the same general trends as that of Leibowitz and Kuo discussed above.

Figure 4 shows that T_e and T_a for nonequilibrium flow are both greater than the equilibrium temperature just behind the shock, whereas, near the body the temperature is essentially the same for equilibrium and non-equilibrium flow. Thermal equilibrium occurs at about $\eta = 0.7$ and the equilibrium and non-equilibrium solutions yield about the same temperature for values of η less than 0.2.

Figure 5 shows that the electron density increases very slowly behind the shock for finite rate ionization (nonequilibrium) as compared to the equilibrium solution. This is an important difference between the two cases when radiative emission is considered, because the electron population is very important in the radiation transfer. Also, for finite rate ionization the atomic hydrogen population is much higher just behind the shock than the equilibrium hydrogen population.

Figure 6 shows typical values of the shock layer optical thickness for the solutions shown in Table 2 as a function of photon energy $h\nu$. In general, the shock layer is optically thin in the spectral region from 1 to 9 ev. It is optically thick at the Lyman line at about 10 ev and for the Lyman continuum, at energies greater than 13.6 ev. The shock layer also becomes optically thick for free-free continuum radiation at very low values of photon energy. The
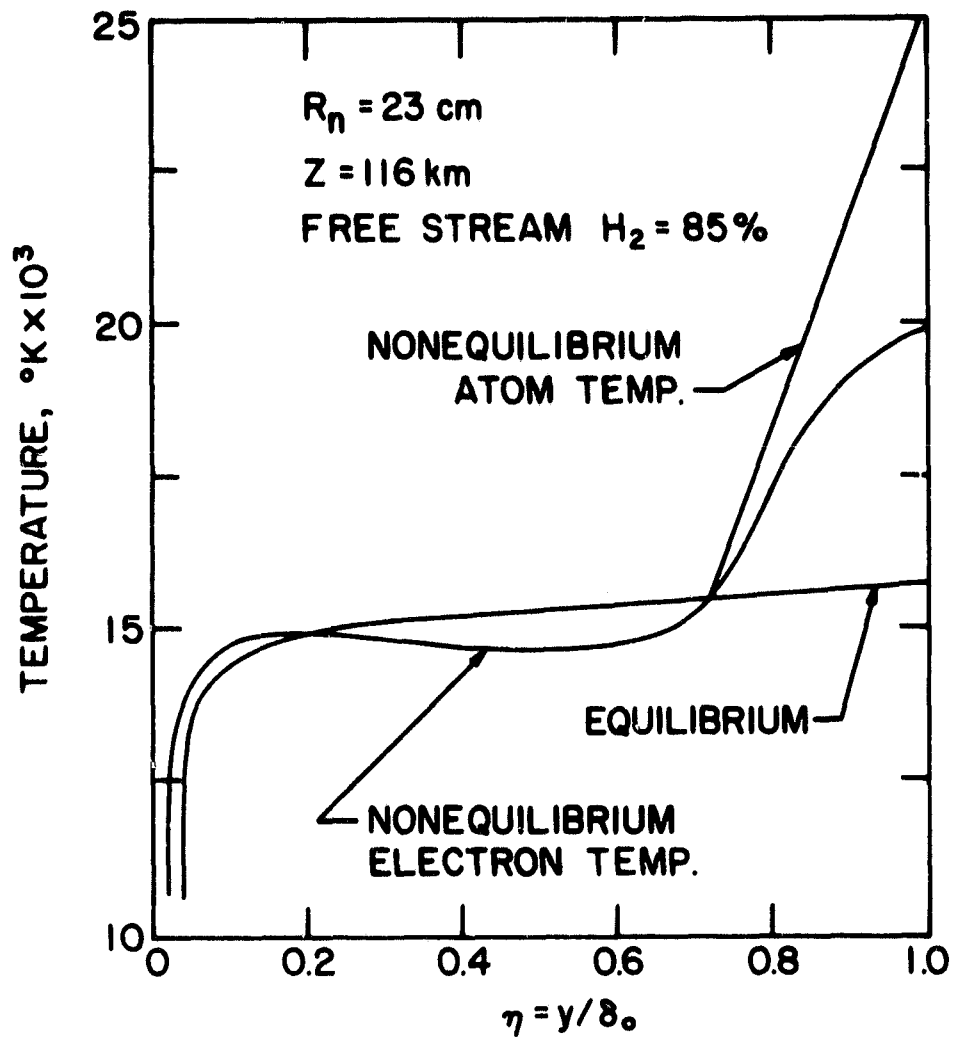
Figure 4.   Temperature Variation in Stagnation Shock Layer
for Equilibrium and Finite Rate Ionization.
(From Ref. 4)
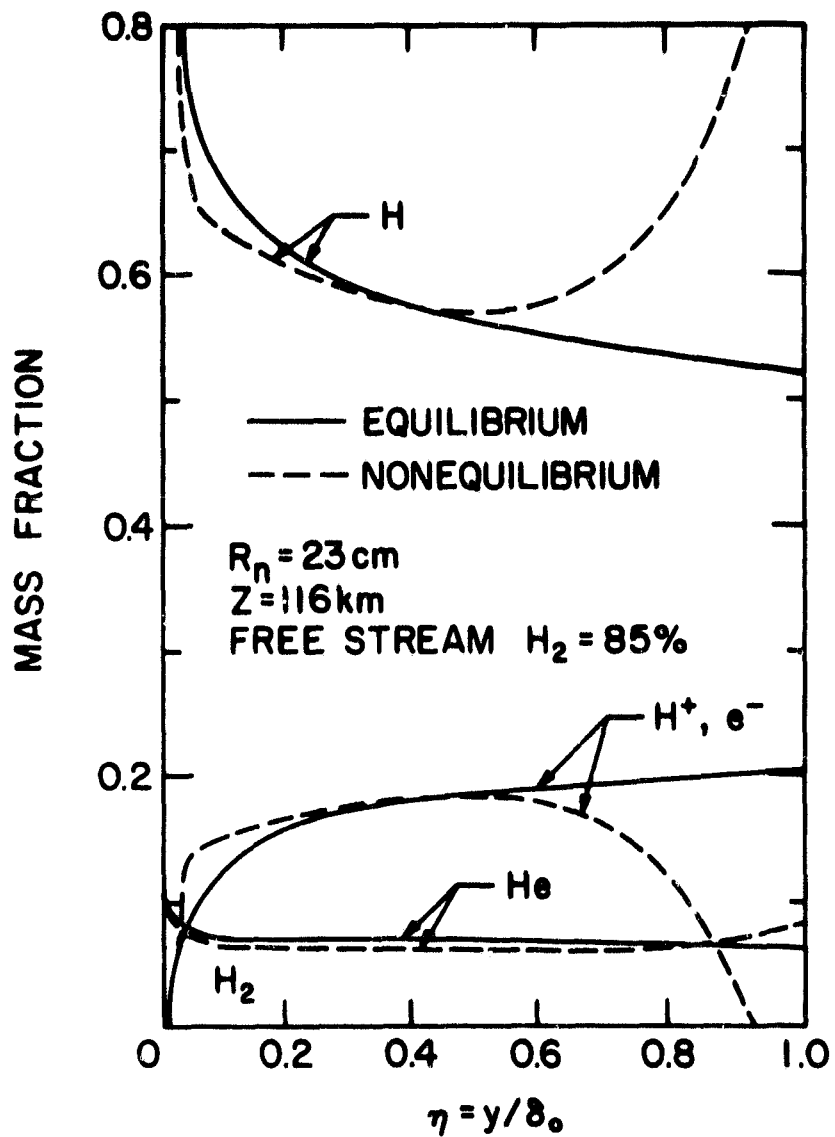
Figure 5. Species Mass Fraction Variation as a Function of Nondimensional Position across the Stagnation Shock Layer. (From Ref. 4)
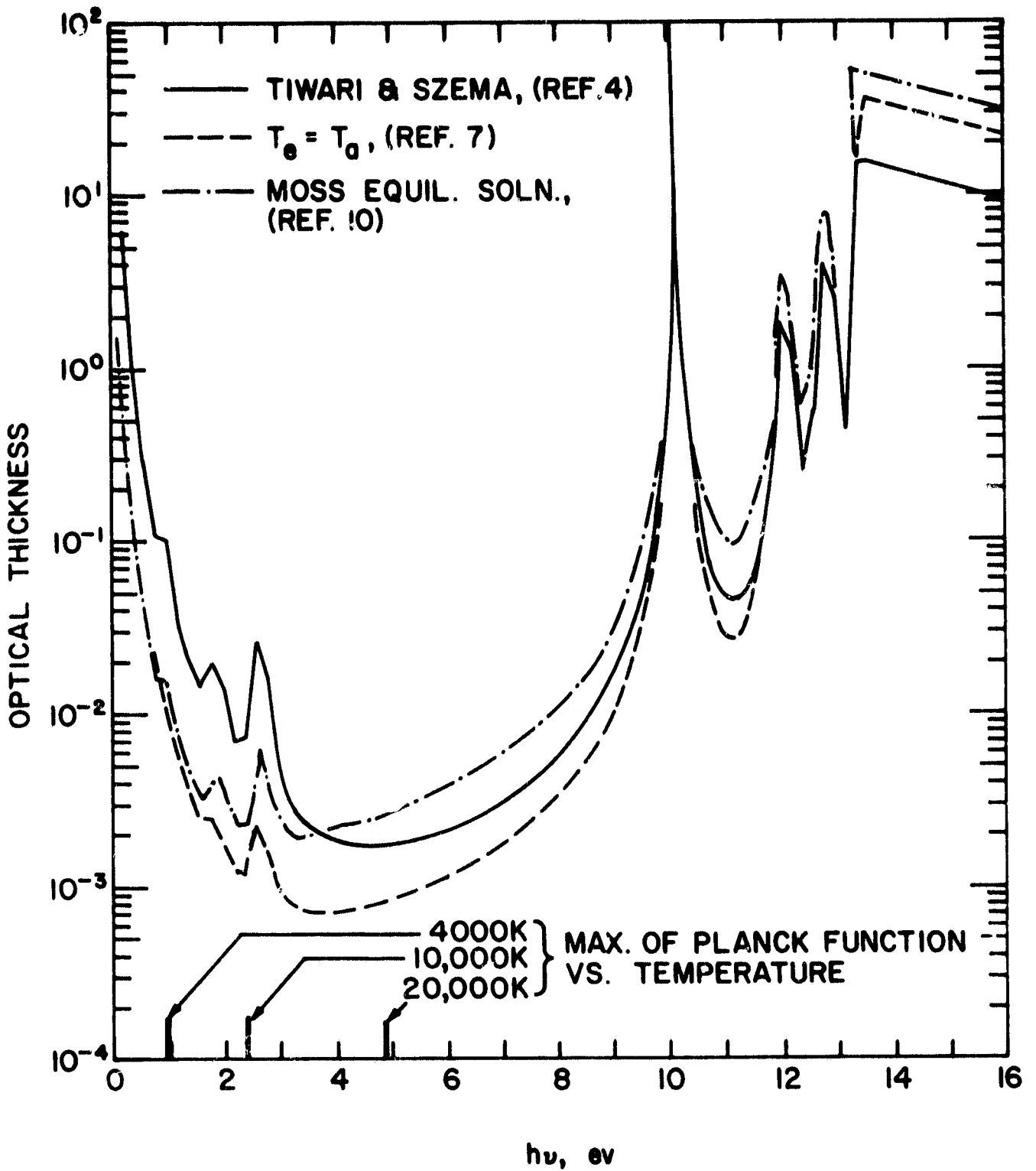
Figure 6. Optical Thickness of the Stagnation Shock Layer as a Function of Radiation Energy.

lower part of Figure 6 shows the spectral position of the maximum of the Planck function as a function of temperature. For the temperatures in the shock layer the maximum occurs in the spectral region where the hydrogen shock layer is optically thin. Thus, when the radiation source function is the Planck function, most of the radiation emitted just behind the shock can easily reach the body.

Figure 7 shows the equilibrium and finite rate ionization radiative heat flux toward the body as a function of nondimensional position in the shock layer for the second case listed in Table 2. For the equilibrium ionization case the majority of the radiative emission occurs relatively close to the body at about $\eta = 0.2$. In the finite ionization rate calculations the most intense radiative emission occurs near the shock wave at about $\eta = 0.9$. This difference can be explained by considering the radiation source function and the optical thickness in the shock layer.

Radiative Flux at the Body

The radiative flux reaching the body involves an integral over the source function (see eqs. (40) and (41), Appendix B).

$$q_R(0,\nu) = -2\pi \int_{-1}^{0} \int_{0}^{\tau_\nu^1} S_\nu(t_\nu) \exp[t_\nu/\mu] \, dt_\nu \, d\mu. \tag{12}$$

Using the tangent-slab approximation, Eq. (12) can be integrated over μ to yield

$$q_R(0,\nu) = -2\pi \int_{0}^{\tau_\nu^1} S_\nu(t_\nu) E_2(t_\nu) dt_\nu \tag{13}$$

where $E_2(t_\nu)$ is the Exponential Integral of order 2. The source function $S_\nu(t_\nu)$ and the absorption coefficient τ_ν are functions of the electron temperature and the electron and excited state populations as shown by Eqs. (10) and (11). When τ_ν is small $E_2(\tau_\nu)$ is approximately unity and the radiative flux can be written as
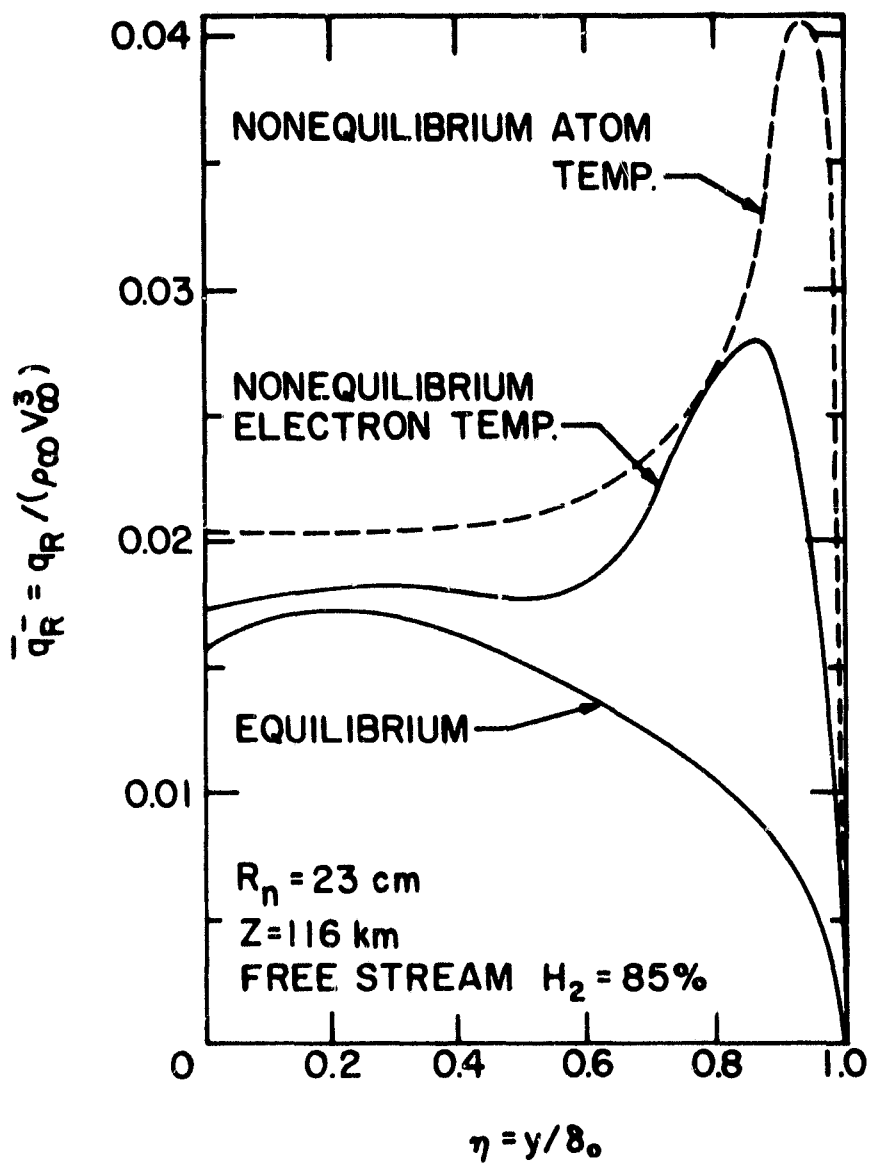
Figure 7. Equilibrium and Finite Rate Ionization Radiative Flux Toward the Body at the Stagnation Point. (From Ref. 4)

$$q_R(0,\nu) = -2\pi \int_0^{\tau_\nu^1} S_\nu(t_\nu) dt_\nu. \tag{14}$$

This relation approximates the radiative flux at the body in the spectral region from 2 to 9 ev, where the shock layers are optically thin. Equation (14) shows that the radiative flux reaching the body is the integral of the source function over the optical radiating volume. It can be written in terms of the shock layer stand-off distance, δ_0 as

$$q_R(0,\nu) = -2\pi \int_0^{\delta_0} S_\nu(\chi) k_\nu(\chi) dy. \tag{15}$$

Thus, the radiative flux at the body is directly related to the radiation source function, the radiative absorption coefficient, and the shock wave stand-off distance when the shock layer is optically thin.

Using Eq. (11) one can rewrite Eq. (15) as

$$q_R(0,\nu) = -2\pi \int_0^{\delta_0} \frac{2h\nu^3}{c^2} \left[[n_a^*(1)_{T_e} \sigma_{1f} + n_a(2)\sigma_{2f}] \exp(-h\nu/kT_e) \right.$$

$$\left. + n_a^*(1)_{T_e} \sigma_{12} \exp\left[\frac{-\chi_{12}(T_a - T_e)}{kT_a T_e}\right] \exp(-h\nu/kT_a) \right] dy, \tag{16}$$

where it is assumed that the excited states and electrons are in equilibrium at T_e. Care must be taken in considering Eqs. (16) because σ_{1f}, σ_{2f} and σ_{12} are functions of the radiation energy. In the optically thin spectral region of the shock layer (approximately 2 to 9 ev) σ_{1f} is zero. Also, one expects σ_{12} to be small in this spectral region because it is mainly in the line wing. Therefore, one can write the radiative flux as

$$q_R(0,\nu) = -2\pi \int_0^{\delta_0} \frac{2h\nu^3}{c^2} n_a(2)\sigma_{2f} \exp(-h\nu/kT_e) dy. \tag{17}$$

Thus, the radiative flux is strongly dependent on T_e and $n_a(2)$. The value of σ_{2f} for hydrogen from page 265 of Reference 11 is

$$\sigma_{2f} = 15.8 \times 10^{-18} (h\nu_2/h\nu)^3 \text{ cm}^2 \tag{18}$$

where $h\nu_2$ is 3.4 ev for hydrogen and $h\nu$ is the photon energy in ev units.

Tiwari and Szema assumed the source function to be the Planck function in their analysis. In addition, the absorption coefficient was determined using equilibrium populations for the atomic electronic states. In their computer code the absorption coefficient was calculated from the number densities for atomic hydrogen, ionized hydrogen, and the electrons at the local temperature. They used a 58-step spectral model developed by Sutton[12], which automatically assumed that the atomic electronic states were Boltzmann populated at the given temperature. For the thermal nonequilibrium, finite ionization rate cases they used the electron temperature to evaluate the source function and absorption coefficient. These assumptions are equivalent to writing the absorption coefficient from Eq. (10) as

$$k_\nu = n_a(2)\sigma_{2f}[1 - \exp(-h\nu/kT_e)] \tag{19}$$

and the source function from Eq. (11) as

$$S_\nu = \frac{2h\nu^3}{c^2} \frac{e^{-h\nu/kT_e}}{1 - e^{-h\nu/kT_e}}, \tag{20}$$

where Eqs. (19) and (20) only apply to the optically thin region of the shock layer. Further, Eq. (17) for the radiative flux at the body can be rewritten using Eqs. (19) and (20) as

$$q_R(0,\nu) = -2\pi \int_0^{\delta_o} \frac{2h\nu^3}{c^2} n_a(2)\sigma_{2f} e^{-h\nu/kT_e} \, dy. \tag{21}$$

Equation (21) points out the strong dependence of the radiative flux on the excited state population and the electron temperature.

In the finite rate ionization solutions of Tiwari and Szema, T_e is high behind the shock as can be seen from Fig. 4. This increases the exponential term of Eq. (21). High values of T_e also increase $n_a(2)$, because they assumed that the electronic state population is Boltzmann distributed at T_e. Thus, the finite rate ionization solutions produce a large radiative flux.

In the equilibrium case the temperature is smaller just behind the shock, as shown in Fig. 4. This reduces the value of the exponential term in Eq. (21). In addition, the number of hydrogen atoms is much lower than it is for the finite ionization rate case (see Fig. 5). Both of these effects reduce the excited state population. Consequently, the contribution of the gas near the shock to the radiative flux is reduced, compared to the finite ionization case. Near the body T_e and $n_a(2)$ are about the same for equilibrium and finite rate ionization; therefore, the radiative flux from this part of the shock layer will be about the same for both assumptions. Thus, the overall magnitude of the equilibrium ionization radiative flux is less than the finite rate ionization radiative flux.

The discussion to this point has been limited to the optically thin approximation and the Balmer region of the spectrum. However, the conclusions are generally valid. As can be seen from Fig. 6 the ground state continuum radiation is optically thick so only gas near the body contributes to radiative heating of the body in that spectral region. The atomic line transitions are also optically thick near the line center, which means that the spectral regions near the line centers will contribute to radiative heating of the spacecraft only if the radiation is emitted close to the body. The free-free continuum transitions occur mainly in the spectral range below 2 ev. The free-free continuum radiation can be important; however, at the temperatures of interest its

contribution to the flux will be small, because of its small source function. Consequently, the radiative heating comes mainly from the Balmer region of the spectrum where the shock layer is optically thin and the above approximations hold.

General Discussion

The physical problem Tiwari and Szema[3,4] solved is one in which the hydrogen atoms have a Boltzmann population distribution of their electronic states at the local electron temperature. The ionization rate was allowed to be finite by using the rate equations developed by Leibowitz[1]. They interpreted the excitation rates in the ionization model as given in Table 1, reactions 3, 4, 5 and 6, as ionization rates. Also, they did not assume the excited states and electrons to be in equilibrium at the electron temperature as Leibowitz did. Leibowitz used the excitation rate as the ionization rate limiting step in a two step ionization model. Once the electrons were excited the number of electrons that became free was determined by the Saha equilibrium condition at the local electron temperature.

In the Leibowitz ionization model the excited state is populated at a finite rate. Thus, its population will lag its local equilibrium value. This implies that the excited state is not populated at its Boltzmann distribution value at the local temperature. Also, the excited state population and the electron population are assumed to be in equilibrium with each other at the electron temperature. Therefore, the excitation rate is not equal to the ionization rate. Both of these effects influence the radiation transfer, because the excited state population distribution influences both the absorption coefficient (Eq. 10)) and the radiation source function (Eq. (11)). In addition, Tiwari and Szema used the Planck function for the source function throughout the shock layer. As is pointed out above, the source function is equal to the Planck function only when the gas is in equilibrium.

31

Table 3 illustrates the difference in the population of the first excited state of hydrogen for the assumption of a Boltzmann population distribution at the electron temperature and for the assumption of the excited state population being in equilibrium with the electron population at the electron temperature. The data for T_e, n_H, and n_e just behind the shock wave was obtained from the solution of Tiwari and Szema shown in Figures 4 and 5. Note that for the Boltzmann distribution the excited state population is much greater than it is for the assumption that the excited states and electrons exist in equilibrium together at the local electron temperature.

The radiation absorption coefficient subroutine used by Tiwari and Szema[3,4] automatically used the Boltzmann distribution for the excited states population. This greatly increased the absorption coefficient compared to its value for the assumption that the excited state population is in equilibrium with the electron population at the electron temperature. This effect together with the high electron temperature just behind the shock compared to the temperature for equilibrium solutions (resulting in a larger value for the radiation source function) increased the radiative emission and is the reason that Tiwari and Szema calculate increased radiation in the finite rate ionization case.

TABLE 3. Population of the first excited state of Atomic Hydrogen assuming:
1) Boltzmann distribution at T_e and 2) excited state in equilibrium
with electrons at T_e. (Tiwari and Szema solution)

η	T_e	n_H	n_e, n_{H^+}	$n_H(2)$*	$n_H(2)$**
	°K	$1/cm^3$	$1/cm^3$	$1/cm^3$	$1/cm^3$
1.000	20,000	8.39×10^{17}	4.66×10^{15}	7.93×10^{15}	9.14×10^{10}
.950	19,500	8.49×10^{17}	9.99×10^{15}	7.67×10^{15}	4.59×10^{11}
.900	19,100	8.22×10^{17}	3.64×10^{16}	6.57×10^{15}	6.57×10^{12}
.875	18,700	8.26×10^{17}	6.6×10^{16}	5.79×10^{15}	2.33×10^{13}
.850	18,400	8.16×10^{17}	8.62×10^{16}	5.17×10^{15}	4.21×10^{13}
.825	18,000	8.19×10^{17}	1.34×10^{17}	4.51×10^{15}	1.11×10^{14}
.800	17,000	8.20×10^{17}	1.53×10^{17}	3.08×10^{15}	1.77×10^{14}

* $n_H(2)$ Boltzmann Population at T_e

** $n_H(2)$ In equilibrium with electrons at T_e

SUMMARY AND CONCLUSIONS

Currently there is disagreement as to whether the cold wall radiative heating for probes entering the atmospheres of the major planets increases or decreases relative to its equilibrium value when finite rate ionization is considered. Leibowitz and Kuo[2] predicted that finite rate ionization in the hydrogen gas just behind the shock wave will reduce the radiative heating; however, Tiwari and Szema[3,4] asserted that it will increase the radiation heating.

The present study investigated the radiation modeling used in each of the above mentioned investigations. It is shown that the radiation transfer analysis used by Tiwari and Szema[3,4] over predicts the radiation emission because they assumed a Boltzmann population distribution at the local electron temperature (which is higher than the equilibrium solution temperature just behind the shock) for the population of the electronic states of atomic hydrogen. This equilibrium population assumption changed the nonequilibrium radiative source function to the Planck function. In addition, it also influenced the atomic radiation absorption coefficient or both line and continuum radiation through the excited state population. Both of these effects increased the local radiation emission just behind the shock wave in the 2 to 9 ev region of the spectrum, where the shock layer is optically thin. This, in turn, increased the radiative heat transfer to the body as compared to equilibrium chemistry predictions.

The more realistic and generally accepted assumption is that the excited states and electrons exist together in equilibrium at the local electron temperature. This is the assumption used by Leibowitz[1] in the development of the hydrogen ionization model. In the finite rate ionization model, excitation to the first excited state is the rate limiting step. Once the electron is excited it is ionized according to equilibrium conditions at the local thermodynamic state. This implies that the excited states are not populated to their boltzmann values

34

at the local conditions.

Tiwari and Szema interpreted the finite rate excitation reactions in the ionization model as ionization reactions. If they would have correctly used the finite rate ionization model in their analysis they would have calculated smaller excited state populations and a smaller source function in the region just behind the shock wave. These effects would have reduced their finite rate ionization radiative heating predictions to values below those predicted by assuming equilibrium chemistry in the shock layer.

In the near future the finite rate ionization model as developed by Leibowitz should be correctly used in a detailed flow field and radiative heat transfer analysis like that of Tiwari and Szema. The results of such an investigation need to be available as "benchmark" solutions. Simplified solutions which make use of the optically thin shock layer assumption and are computationally fast need to be developed and compared to the "benchmark" solutions. Once they are developed, the numerically fast, finite ionization rate schemes need to be upgraded to include the effects of ablation of the wall. The ablation products should be allowed to have finite chemistry and non-Boltzmann populations of their electronic and/or vibrational states. These effects should be included in predictions of the radiation heat transfer to probes entering the atmospheres of the outer planets. The radiative heating predictions need to be as accurate as possible, because the heat shield mass on these missions are very critical. One does not want to over predict the size of the heat shield because of the weight penalty. Yet if one under predicts the size of the heat shield the probe may burn up before it completes its mission.

REFERENCES

1. Leibowitz, L. P., "Measurements of the Structure of an Ionizing Shock Wave in a Hydrogen-Helium Mixture," Phys. Fluids, 16, 59, 1973.

2. Leibowitz, L. P. and Kuo, Ta-Jin, "Ionizational Nonequilibrium Heating During Outer Planetary Entries," Am. Inst. Aeronaut. Astronaut. J., 14, 1324, 1976.

3. Tiwari, S. N. and Szema, K. Y., "Effects of Precursor Heating on Chemical and Radiative Nonequilibrium Viscous Flow Around a Jovian Entry Body," Am. Inst. Aeronaut. Astronaut. Paper No. 78-907, 1978.

4. Tiwari, S. N. and Szema, K. Y., "Effects of Precursor Heating on Radiating and Chemically Reacting Viscous Flow Around a Jovian Entry Body," NASA CR-3186, September 1979.

5. Howe, J. T., "Hydrogen Ionization in the Shock Layer for Entry into the Outer Planets," Am. Inst. Aeronaut. Astronaut. J., 12(6), 875-876, June 1974.

6. Stickford, G. H., "Total Radiative Intensity Calculations for 100% H_2 and 87% H_2 - 13% H_3," J. Quant. Spect. Rad. Transfer, 12, 525-529, 1972.

7. Zoby, E. V. and Moss, J. N., "Preliminary Thermal Analysis for Saturn Entry," Am. Inst. Aeronaut. Astronaut. Paper No. 80-0359, January 1980.

8. Nelson, H. F. and Goulard, R., "Structure of Shock Waves with Nonequilibrium Radiation and Ionization," Phys. Fluids, 12, 1605, 1969.

9. Leibowitz, L. P., Menard, W. A. and Stickford, G. H., "Radiative Relaxation Behind Strong Shock Waves in Hydrogen-Helium Mixtures," Proceedings of the Ninth International Shock Tube Symposium, Edited by D. Bershader and W. Griffith, 306, 1973.

10. Moss, J. N., "A Study of the Aerothermal Entry Environment for the Galileo Probe," AIAA Paper 79-1081, 1979.

11. Zel'dovich, Ya. B., and Raizer, Yu. P., Physics of Shock Waves and High-Temperature Hydrodynamic Phenomena, Academic Press, New York, N.Y., 1966.

12. Zoby, E. V., Sutton, K., Olstad, W. B. and Moss, J. N., "An Approximate Inviscid Radiating Flow-Field Analysis for Outer Planet Entry Probes," AIAA Paper 78-189, 1978.

13. Losev, S. A. and Osipov, A. I., "The Study of Nonequilibrium Phenomena in Shock Waves," Soviet Physics USPEKHI, [Russian, Vol. 74, Nos. 3-4], January-February 1962.

14. Biberman, L. M., Vorob'ev, V. S. and Norman, G. E., "Radiative Heating in Hypersonic Flow," Cosmic Research, 2, 376, 1964.

15. Biberman, L. M., Vorob'ev, V. S., Lagar'kov, A. N., Stulov, V. P., Telenin, G. F., Sharpiro, E. G. and Iakubov, I. T., "Air Flow Behind a Strong Shock Front Taking Account of Nonequilibrium Ionization and Radiation," Izv. AN SSSR, Mekhanika Zhidk. i Gaza, No. 6, 46-57, 1967.

16. Biberman, L. M., Mnatsakanyan, A. Kh., Yakubov, I. T., "Ionization Relaxation Behind Strong Shock Waves in Gases," Soviet Physics USPEKHI, 13, No. 6, 728, 1971.

17. Bond, J. W., Watson, K. M. and Welch, J. A., Atomic Theory of Gas Dynamics, Addison-Wesley, Reading, Mass., 1965.

18. Heaslet, N. A. and Baldwin, B. S., "Predictions of the Structure of Radiation Resisted Shock Waves," Phys. Fluids, 6, 781, 1963.

19. Cohen, I. M. and Clarke, J. H., "Influence of Viscosity on Shock Waves Structured by Radiation," Phys. Fluids, 8, 1278, 1965.

20. Chow, R. R., "Effect of Thermal Radiation on Thin Shock Structure," AIAA J., 3, 973, 1965.

21. Traugott, S. C., "Shock Structure in a Radiating Heat Conducting and Viscous Gas," Phys. Fluids, 8, 834, 1965.

22. Sen, H. K. and Guess, A. W., "Radiation Effects in Shock Wave Structure," Phys. Rev., 108, 560, 1957.

23. Petschek, H. E., Rose, P. H., Glick, H. S., Kane, A., and Kantrowitz, A., "Spectroscopic Studies of Highly Ionized Argon Produced by Shock Waves," J. Appl. Phys., 26, 83, 1955.

24. Redkoboradyi, Yu. N. and Fedulov, V. I., "Bolometer Measurement of Emission from Argon Ionized by a Shock Wave," Sov. Phys, Tech. Phys., 10, 1275, 1960.

25. Oettinger, P. E. and Bershader, D., "A Unified Treatment of the Relaxation Phenomenon in Radiating Argon Plasma Flows," AIAA Journal, 5, 1625, 1967.

26. McChesney, M. and Al-Attar, Z., "Continuum Radiation Losses in Shock Heated Argon," JQSRT, 5, 553, 1965.

27. Pomerantz, J., "The Influence of the Absorption of Radiation in Shock Tube Phenomena," JQSRT, 1, 185, 1961.

28. Yoshikawa, K. K. and Chapman, D. R., "Radiative Heat Transfer and Absorption Behind Hypersonic Normal Shock Waves," NASA TN D-1424, 1962.

29. Petschek, H. H. and Byron, S., "Approach to Equilibrium Ionization Behind Strong Shock Waves in Argon," Ann. Phys. (New York), 1, 270, 1957.

30. Kamimoto, G. and Teshima, K., "Study on Ionizing Shock Waves in Argon: I: Precursor Phenomena," Transactions Japan Society for Aeronautical and Space Sciences, 15, 124, 1972.

31. Kamimoto, G. and Teshima, K., "Study on Ionizing Shock Waves in Argon: II: Ionization Relaxation," Transactions Japan Society for Aeronautical and Space Sciences, 15, 141, 1972.

32. Kamimoto, G. and Teshima, K., "Study on Ionizing Shock Waves in Argon: III: Thermodynamic Properties of the Plasma," Transactions Japan Society for Aeronautical and Space Sciences, 15, 183, 1973.

33. Wong, H. and Bershader, D., "Thermal Equilibrium Behind an Ionizing Shock," J. Fluid Mech., 26, 459, 1966.

34. Horn, K. P., Wong, H. and Bershader, D., "Radiative Behavior of a Shock-Heated Argon Plasma Flow," Journal of Plasma Physics, 1, 157, 1967.

35. Glass, I. I. and Liu, W. S., "Effects of Hydrogen Impurities on Shock Structure and Stability in Ionizing Monatomic Gases: Part 1. Argon," J. Fluid Mech., 84, 55, 1978.

36. Golobic, R. A. and Nerem, R. M., "Structure of Strong Shock Waves in Xenon, I: Electron Temperature Measurements," Phys. Fluids, 16, 1622, 1973.

37. Foley, W. H., Bader, J. B. and Nerem, R. M., "Structure of Strong Shock Waves in Xenon, II: Further Experiments and Theoretical Interpretation," Phys. Fluids, 16, 1630, 1973.

38. Belozerov, A. N. and Measures, R. M., "The Initial Ionization of Hydrogen in a Strong Shock Wave," J. Fluid Mech., 36, 695, 1969.

39. Stalker, R. J., "Shock Tunnel Measurement of Ionization Rates in Hydrogen," AIAA Journal, 18, 478, 1980.

40. Biberman, L. M. and Yakubov, I. T., "Approach to Ionization Equilibrium Behind the Front of a Shock Wave in an Atomic Gas," Soviet Physics-Technical Physics, 8, 1001, 1964.

41. Clarke, J. H. and Ferrari, C., "Gas Dynamics with Nonequilibrium Radiative and Collisional Ionization," Physics of Fluids, 8, 2121, 1965.

42. Hoffert, M. I. and Lien, H., "Quasi-One-Dimensional, Nonequilibrium Gas Dynamics of Partially Ionized Two-Temperature Argon," Physics of Fluids, 10, 1769, 1967.

43. Honma, H. and Nakadaira, S., "Ionizing Shock Structure in a Weakly Ionized Gas," Transactions Japan Society for Aeronautical and Space Sciences, 14, 102, 1971.

44. Honma, H., "Electron Energy Transfer Processes in a Weakly Ionized Nonequilibrium Flow," Journal of the Physical Society of Japan, 32, 1300, 1972.

45. Foley, W. H. and Clarke, J. H., "Shock Waves Structured by Nonequilibrium Ionizing and Thermal Phenomena," Phys. Fluids, 16, 375, 1973.

46. Nelson, H. F., "Nonequilibrium Structure of Argon Shock Waves," Phys. Fluids, 16, 2132, 1973.

47. Chubb, D. L., "Ionizing Shock Structure in a Monatomic Gas," Phys. Fluids, 11, 2363, 1968.

48. Murthy, M. K. and Ramachandra, S. M., "Ionizing Shock Waves in Monatomic Gases Through a Kinetic Theory Approach," Acta Astronautica, 2, 367, 1975.

49. Whitney, C. A. and Skalafuris, A. J., "The Structure of a Shock Front in Atomic Hydrogen I: The Effects of Precursor Radiation in the Lyman Continuum," Astrophysical Journal, 138, 200, 1963.

50. Skalafuris, A. J., "The Structure of a Shock Front in Atomic Hydrogen II: The Region of Internal Relaxation," Astrophysical Journal, 142, 351, 1965.

51. Skalafuris, A. J., "The Structure of a Shock Front in Atomic Hydrogen III: The Radiative Relaxation Region," Astrophysics and Space Science, 2, 258, 1968.

52. Skalafuris, A. J., "Radiative Shock Structure - Theory and Observations," J. Quant. Spectrosc. Radiat. Transfer, 8, 515, 1968.

53. Koch, P. A. and Gross, R. A., "Effect of Radiation upon the Post-Shock State," Phys. Fluids, 12, 1182, 1969.

54. Clarke, J. H. and Onorato, M., "Normal Shock Waves Structured by Non-equilibrium Radiative and Collisional Ionization," J. Appl. Mech., 37, 783, 1970.

55. Vinolo, A. R. and Clarke, J. H., "Interrelated Structures of the Transport Shock and Collisional Relaxation Layer in a Multitemperature, Multilevel Ionized Gas," Phys. Fluids, 16, 1612, 1973.

56. Weymann, H. D., "On the Mechanism of Thermal Ionization Behind Strong Shock Waves," Institute for Fluid Dynamics and Applied Mathematics, U. Maryland Tech. Note BN-144, 1958, also AD 202 113.

57. Harwell, K. E. and Jahn, R. G., "Initial Ionization Rates in Shock Heated Argon, Krypton and Xenon," Phys. Fluids, 7, 514, 1964.

58. Kelly, A. J., "Atom-Atom Ionization Cross Sections of the Noble Gases - Argon, Krypton and Xenon," J. Chem. Phys., 45, 1723, 1966.

59. Hacker, D. S. and Bloomberg, H., "Investigation of Early Ionization Processes in Shocked Xenon," J. Chem. Phys., 39, 3263, 1963.

60. Morgan, E. J. and Morrison, R. D., "Ionization Rates Behind Strong Shock Waves in Argon," Phys. Fluids, 8, 1008, 1965.

61. Hey, J. S., Parsons, S. J. and Stewart, G. S., "Radar Observations of the Giacobinal Meteor Shower, 1964," Mon. Not. Roy. Astron. Soc., 107, 176, 1947.

62. McKinley, D. R. W. and Millman, B. M., "A Phenomenological Theory of Radar Echoes from Meteors," Proc. IRE, 37, 364, 1949.

63. Lin, S. C., "Radar Echoes from a Manned Satellite During Re-entry," J. Geophysical Research, 67, 3851, 1962.

64. Serou, P. and Murty, S. S. R., "Ionization Build-up Behind Hypersonic Shock Waves," Journal of Aeronautical Society of India, 24, 231, 1972.

65. Nakagawa, Y. and Wisler, D. C., "Spectroscopic Study of Radiative Shock Structure in Hydrogen," Proceedings of the Seventh International Shock Tube Symposium, Edited by I. I. Glass, 620, 1970.

66. Hollyer, R. N., "Preliminary Studies in the APL High Temperature Shock Tube," Johns Hopkins University, Applied Physics Lab. Rept. CM-903, May 1957.

67. Weymann, H. D., "Electron Diffusion Ahead of Shock Waves in Argon," Phys. Fluids, 3, 545, 1960.

68. Hammerling, P., "Ionization Effects of Precursor Radiation from Shocks in Air," AVCO Everett Research Report 98, June 1960.

69. Gloersen, P., "Some Unexpected Results of Shock-Heating Xenon," Physics of Fluids, 3, 857, 1960.

70. Jones, D. L., "Precursor Electrons Ahead of Cylindrical Shock Waves," Physics of Fluids, 5, 1121, 1962.

71. Groenig, H., "Precursor Photoionization and Electrons," Physics of Fluids, 6, 142, 1963.

72. Zivanovic, S., "Investigation of Precursor Ionization in Front of The Shock Waves of Hypersonic Projectiles," AIAA Preprint, 63-458, August 1963.

73. Valentin, P. and Leboucher, J. C., "Phenomenes Precursors d'ondes de choc dans l'argon," Comptes Rendus (Academic Des Sciences, Paris), Series B, Sciences Physiques, 263, 959, 1966. (In French).

74. Wilson, D. S. and Lederman, S., "Precursor Ionization Due to Photoionization of H_2 Impurities in Argon Shocks," Polytechnic Institute of Brooklyn, PBIAL Report No. 1033, 1967.

75. Mermagen, W. H., "Precursor Infrared Radiation from Hypervelocity Ablating Bodies," Physics of Fluids, 10, 1801, 1967.

76. Lederman, S. and Wilson, D. S., "Microwave Resonant Cavity Measurement of Shock Produced Electron Precursors," AIAA Journal, 5, 70, 1967.

77. Weymann, H. D., "Precursors Ahead of Shock Waves: I. Electron Diffusion," Phys. Fluids, 12, 1193, 1969.

78. Homes, L. B. and Weymann, H. D., "Precursors Ahead of Shock Waves: II Photo-ionization," Phys. Fluids, 12, 1200, 1967.

79. McRae, T. G. and Leadon, B. M., "Observations of Precursor Ionization in Electromagnetic T-Tubes," Phys. Fluids, 13, 2067, 1972.

80. Barach, J. P., "Probe Measurements on a Shock Precursor," Phys. Fluids, 22, 837, 1979.

81. Pipkin, A. C., "Diffusion from a Slightly Ionized Region in a Uniform Flow," Physics of Fluids, 4, 1298, 1961.

82. Wetzel, L., "Precursor Effects and Electron Diffusion from a Shock Front," Physics of fluids, 5, 824, 1962.

83. Pipkin, A. C., "Precursor Waves in Shock Tubes," Physics of Fluids, 6, 1382, 1963.

84. Wetzel, L., "A Feature of Precursor Ionization Profiles due to Shock Radiation," Physics of Fluids, 6, 750, 1963.

85. Lagar'kov, A. N. and Yakubov, I. T., "The Effect of Radiation on the State of a Gas Ahead of a Shock Wave Front," Optics and Spectroscopy, 14, 103, 1963.

86. Wetzel, L., "Far-Flow Approximations for Precursor Ionization Profiles," AIAA Journal, 2, 1208, 1964.

87. Zinman, W. G., "Comment on Experimental Precursor Studies," AIAA Journal, 4, 2073, 1966.

88. Sinclair, M., Sonin, A. A. and De Leeuw, J. H., "Diffusive Separation of Ions and Atoms in a Shock Wave," Physics of Fluids, 10, 891, 1967.

89. Appleton, J. P., "Electrical Precursors of Ionizing Shock Waves," Physics of Fluids, 9, 336, 1966.

90. Wilson, D. S. and Lin, T. C., "Impurity Photoionization Theory of Precursors," Polytechnic Institute of Brooklyn, PBIAL Report No. 1006, 1967.

91. Murty, S. S. R., "Effect of Line Radiation in Precursor Ionization," J. Quant. Spectrosc. Radiat. Transfer, 8, 531, 1968.

92. Vulliet, W. G., "Effect of Resonance Radiation on the Transfer of Shock Precursor Radiation," Phys. Fluids, 11, 1377, 1968.

93. Smith, G. L., "Radiation Induced Precursor Flow Field Ahead of a Reentering Body," AIAA Paper No. 68-667, 1968.

94. Edwards, K. R., "Precursor Plasma Formation for Blunt Re-entry Vehicles," AIAA Paper No. 69-718, 1969.

95. Murty, S. S. R., "Electron Temperature Distribution Across a Shock Wave in a Partially Ionized Gas," Phys. Fluids, 12, 1830, 1969.

96. Dobbins, R. A., "Precursor Photoexcitation and Photoionization of Argon in Shock Tubes," AIAA Journal, 8, 407, 1970.

97. Liu, J. T. C., "Influence of Upstream Absorption on the Inviscid Stagnation Region Shock Layer Radiation," AIAA Journal, 8, 1730, 1970.

98. Pirri, A. N. and Clarke, J. H., "Accuracy of Differential Approximation for Radiative Ionization in Cold Precursor of Axisymmetric Detached Shock," J. Quant. Spectrosc. Radiat. Transfer, 10, 775, 1970.

99. Pirri, A. N. and Clarke, J. H., "Radiative Ionization Patterns in Cold Precursor of Axisymmetric Detached Shock," AIAA Journal, 8, 1574, 1970.

100. Murty, S. S. R., "Electron Number Density at Shock Front due to Precursor Photoionization," AIAA J. 9, 1427, 1971.

101. Zinn, J. and Anderson, R. C., "Structure and Luminosity of Strong Shocks in Air," Phys. Fluids, 16, 1639, 1973.

102. Nelson, H. F., "Analytical Solution for Shock Wave Precursors," AIAA Journal, 13, 115, 1975.

103. Lasher, L. E. and Wilson, K. H., "Effect of Shock Precursor Absorption on Superorbital Entry Heating," AIAA Journal, 6, 2419, 1968.

104. Farnsworth, A. V. and Clarke, J. H., "Radiatively and Collisionally Structured Shock Waves Exhibiting Large Emission-Convection Ratio," Phys. Fluids, 14, 1352, 1971.

105. Oggiano, M. S. and Onorato, M., "Effects of Nonequilibrium Phenomena on the Structure of a Strong Normal Shock," Proceedings of Ninth International Shock Tube Symposium, 761, 1973.

106. Ledoux, P. and Whitney, C. A., "Spherically-Symmetric Motions in Stellar Atmospheres - Pulsating Variable Stars," Proceedings of International Astronomical Union Symposium No. 12, published in Nuovo Cimento Supp. 22, 131, 1961.

107. Kaplan, S. A., Interstellar Gas Dynamics, Translation by Technical Information Center MCLTD, WRight-Patterson AFB, 1959.

108. Evans, J. W., editor, The Solar Corona, (Proceedings of I.A.U. Symposium No. 16) Academic Press, Inc. New York, 1963.

109. Yoshikawa, K. K., "Analysis of Radiative Heat Transfer for Large Objects at Meteoric Speeds," NASA TN D-4051, 1967.

110. Siegel, R. and Howell, J. R., Thermal Radiation Heat Transfer, 2nd Edition, Hemisphere Printing Co., New York, N.Y., 1981, Chapters 13 and 16.

111. Sonntag, R. E. and Van Wylen, G. J., Introduction to Thermodynamics: Classical and Statistical, John Wiley & Sons, New York, N.Y., 1971, Chapter 19.

112. Jefferies, J. T., Spectral Line Formation, Blaisdell Publishing Co., Waltham, Mass., 1968.

APPENDIX A: REVIEW OF NONEQUILIBRIUM SHOCK WAVE STRUCTURE

This section is devoted to a survey of the conclusions and results of theoretical and experimental studies of the relaxation phenomena in shock waves and the shock wave precursors. Relaxation phenomena behind shock waves have been discussed in reviews and monographs[11,13-17]. This section contains a discussion of the research conducted on the relaxation and precursors of non-equilibrium shock waves. This section does not contain an exhaustive account of all the research conducted on shock wave structure, but rather presents a discussion of the background experiments and theory leading to the present state of knowledge.

Figure A-1 shows a schematic of the nonequilibrium shock wave structure for an atomic gas. It is typical of shock waves advancing at Mach numbers from 10 to 40, into a gas at 300 K and 1 cm Hg pressure. Just behind the shock wave there is a collision dominated relaxation region, wherein the shocked gas relaxes to its thermal and chemical equilibrium state. In the equilibrium region the gas cools due to the emission of radiation. Some of the radiation emitted behind the shock wave propagates into the region in front of the shock wave, where it is absorbed by the cold gas to form the precursor. The degree of excitation and ionization in the precursor is coupled to the relaxation region through the radiation transfer.

Relaxation Region Shock Structure in Atomic Gases

Strong shock waves and high radiative heating rates that occur during the entry into the atmospheres of the outer planets have created a need to improve our understanding of the effects of the radiation, and collision processes in the relaxation process behind the shock wave. The hot gas radiative energy can propagate through the viscous shock wave and be partially absorbed by the cold gas in front of it. This absorbed radiation is referred to as trapped radiation.
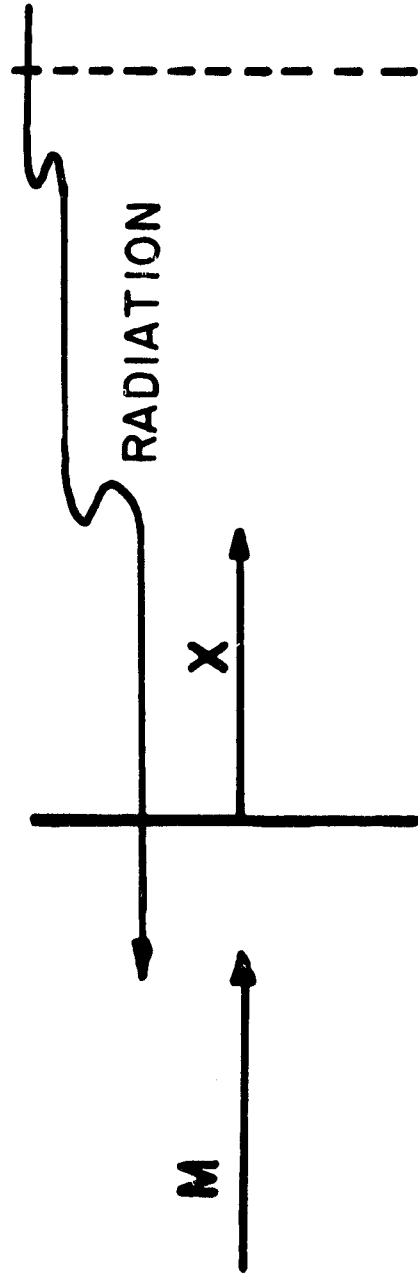
Figure A-1. Nonequilibrium Shock Wave Structure.

The absorption of this energy heats, excites and ionizes the cold gas; there-fore, the shock wave propagates into an excited and ionized media. This pre-ionization and preexcitation can influence the approach to equilibrium in the relaxation region behind the shock and the heat transfer to the entry vehicle. The radiation which is not absorbed by the cold gas is lost, and is referred to as radiation cooling.

Heaslet and Baldwin[18] have obtained solutions for shock waves propagating in a perfect grey gas in which all of the radiation is trapped. The nature of their solution depends on the amount of radiative heating compared to viscous dissipation. If radiative heating exceeds viscous heating, it is possible to have a shock with no discontinuities. When radiative heating is less than viscous heating, the shock has a discontinuity produced by viscous dissipation which is embedded within a larger inviscid region. Cohen and Clarke[19] and Chow[20] have shown that this is a valid model of the shock wave, if the pene-tration length of the radiation is large compared to the extent of the viscous region. Solutions for shock waves with combined radiation and viscosity with no restriction on the size of the penetration length have been obtained by Traugott[21]. Sen and Guess[22] also solved the combined problem, but employed the Rosseland approximation to calculate the radiation transport in the shock wave.

Radiation cooling effects have been observed in shock tube experiments by Petschek, et. al.[23], Redkoboradyi and Fedulov[24], and Oettinger and Bershader[25]. McCheshney and Al-Attar[26] and Petschek, et. al.[23], made calculations of radiation cooling assuming the shocked gas to be optically thin. Solutions including self-absorption effects have been obtained by Pomerantz[27] and Yoshikawa and Chapman[28].

Ionization Relaxation

Considerable information is available in the literature on the relaxation

of atomic gases behind strong shock waves. Most of the analysis has been done for shock tube ambient conditions of about 0.001 atmosphere pressure, 300 K and Mach numbers from 10 to 40. Experimental results have been obtained using argon [25,29-35], xenon [36,37] and hydrogen [1,38,39] as the test gases. Numerical results for the ionization relaxation are available for shocks in argon [8,40-46], xenon [47,48], hydrogen [49-53] and helium [54,55].

Ionization proceeds in a very complicated way behind shock waves in atomic gases. Petschek and Byron [29] showed that more than one ionization process was necessary to reach equilibrium ionization. If the electron concentration is sufficiently high, electron-atom collisions are the most probable ionization process. Petschek and Byron measured the electron-atom ionization rate. Their ionization rate was consistent with a two-step reaction scheme consisting of excitation followed by ionization of the excited state.

$$e + A \rightarrow A^* + e,$$
$$e + A^* \rightarrow A^+ + e + e.$$
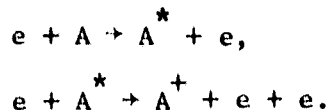
Furthermore, their measurements showed that the electrons were not in thermal equilibrium with the atoms during the ionization process. This occurred be-cause the electrons gained energy by collisions with heavy particles less ef-ficiently than they lost energy by creating ions. Thus, ionization by electron-atom collisions resulted in a net loss of energy in the electron gas, which then became colder than the atom gas. Thus, the gas behind the shock wave can be assumed to exist as two separate gases: the electron gas and the heavy particle (atom) gas. The electrons establish equilibrium among themselves at the electron temperature while the atoms and ions establish equilibrium among themselves at the atom temperature. Consequently, thermal nonequilibrium will exist in the relaxation region.

During the early stages of ionization the electron concentration is too

small to support ionization by electron-atom collisions. Petschek and Byron speculated that reactions involving atom-atom collisions, radiation, and contaminants contributed to the ionization in this region. Weymann[56] theorized that the most probable atom-atom reaction would be a two-step reaction similar to the two-step electron-atom reaction.

$$A + A \rightarrow A^* + A,$$
$$A^* + A \rightarrow A^+ + e + A.$$

This reaction was experimentally verified by Harwell and Jahn[57]. Impurity levels had to be reduced to a few parts per million before their effects became negligible. The experiment was further refined by Kelly[58] who confirmed and improved the results of Harwell and Jahn.

The effects of contaminant reactions have been investigated in xenon shock waves by Hacker and Bloomberg[59]. They found a very complicated set of reactions involving contaminant species and xenon atoms in various stages of excitation, and radiation. Contaminant reactions in argon were theoretically discussed by Morgan and Morrison[60].

Radiation can be important in the ionization process too. Bibermann and Yakubov[40] have shown that line radiation from the region following the region of nonequilibrium ionization excites argon atoms in the nonequilibrium ionization region. The excited atoms are easily ionized and contribute additional electrons, which reduces the time to reach equilibrium. Radiation can affect the ionization by creating electrons ahead of the shock front. Such precursor electrons have been observed in a re-entry by their effect on radar cross section[61-63] and in shock tubes is described below.

In a series of papers, Skalafuris[49-52] investigated the structure of a shock wave in atomic hydrogen. His analysis was done for conditions that exist in stellar atmospheres rather than shock tube, or planetary atmospheric entry. He

considered shock waves traveling at 30 to 70 km/sec into un-ionized atomic hydrogen at a temperature of 5000 K, for a range of densities from 10^{-9} to 10^{-10} gm/cm^3, which corresponds to a pressure range of 4×10^{-5} to 4×10^{-4} atm. The results show the same trends as those in argon, in that the Lyman radiation is important in forming the precursor, the precursor raises the gas temperature behind the shock, the collisional relaxation region behind the shock is optically thin to Lyman and Balmer radiation and that the electron temperature is less than the heavy particle temperature in the relaxation region.

A general model for nonequilibrium shock wave structure in atomic gases, including both collisional and radiative processes, has evolved. It consists of a radiation induced precursor, and embedded viscous shock, an inner collisional relaxation region and an outer radiation cooling region as shown in Figure A-1.

The relaxation mechanism to ionizational equilibrium occurs in two stages. The first is due to atom-atom collisions and the second is due to electron-atom collisions. Thus, one expects a region just behind the shock where the electronic state excitation and the ionization are produced by atom-atom collisions. When the number of free electrons becomes significant the electron-atom collisions rapidly drive the excitation and ionization to equilibrium. Throughout most of the relaxation region the heavy particles are at a higher temperature than the electrons because the electrons lose energy through ionization collisions faster than they gain energy by elastic collisions with the atoms. The nonequilibrium gas usually reaches thermal equilibrium just prior to attaining ionizational equilibrium.

A model has evolved for the excitation and subsequent ionization of atoms. Most atomic gases have a large energy difference between the ground electronic state and the first excited state compared to the energy difference between the first excited state and ionization as shown schematically in Fig. A-2 for an
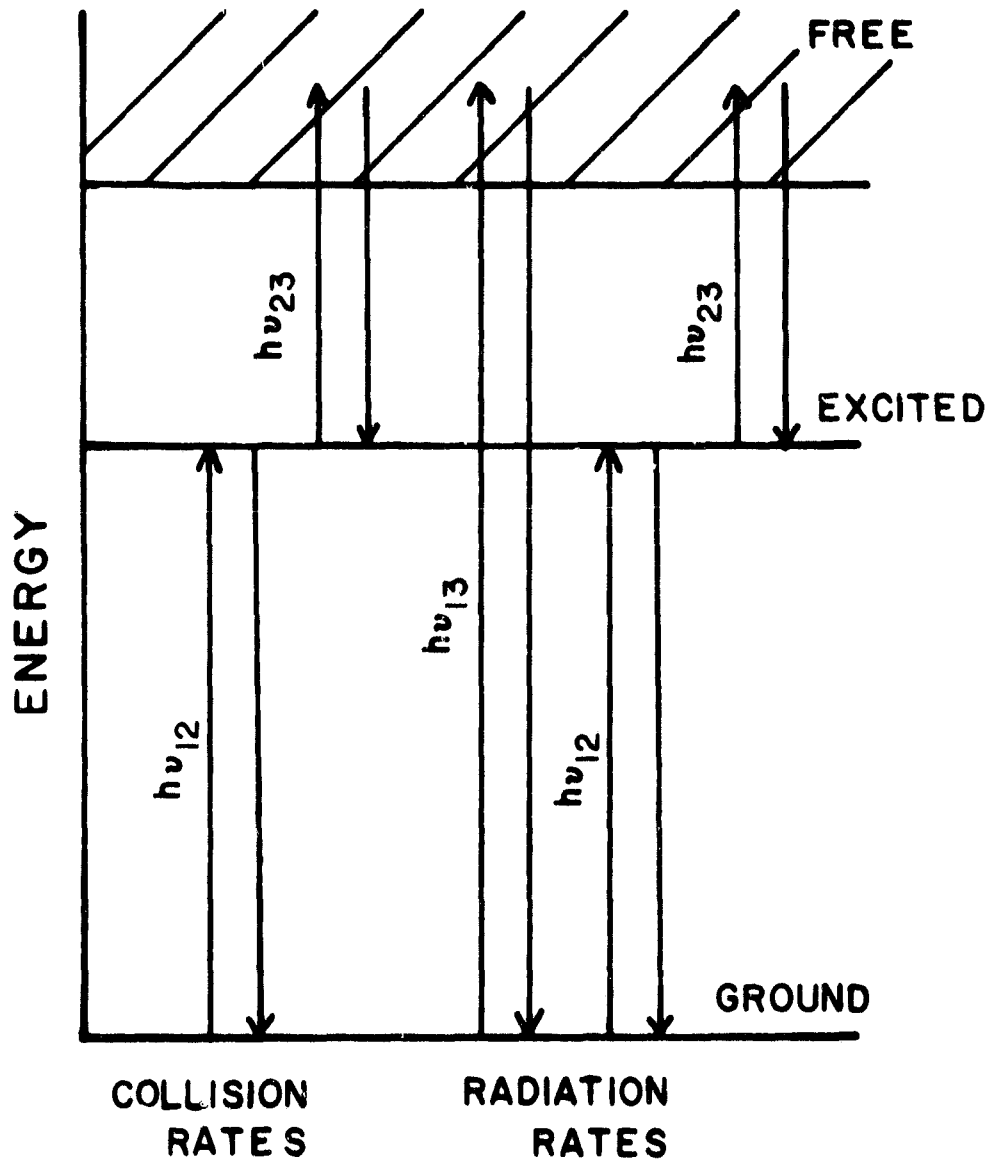
Figure A-2. Atomic Transitions.

atom with two electronic states. The electrons and excited electronic states are very close to each other in energy; consequently, they are assumed to exist together in equilibrium at the electron temperature. In an experimental study, Leibowitz, et. al.[9] found that most of the excited atomic electronic states were in equilibrium with the free electrons and were at the free electron temperature.

It has been shown experimentally that the rate of ionization is controlled by the rate of excitation between the ground state and the first excited state. Once the electron is excited to the first excited state it will rapidly ionize. Thus, the collisional ionization occurs as a two-step process as shown in Fig. A-2. In atomic gas shock wave structure studies it is acceptable to assume that the excited state population is in equilibrium with the electron population at the electron temperature and that the ionization rate is controlled by the excitation rate between the ground and first excited state.

Nonequilibrium Shock Wave Structure in Hydrogen-Helium

Belozerov and Measures[38] theoretically and experimentally investigated the initial ionization process in strong shock waves in hydrogen. Their analysis indicated that the electron temperature and atom temperature were essentially equal throughout the relaxation region. This appears to be in error due to the use of an incorrect value of the elastic atom-electron collision cross section[64]. Leibowitz[1] obtained results that agree with Belozerov and Measures when he increased the elastic electron-atom cross section to the value used by them. Thus, T_e should be less than T_a through most of the relaxation region as occurs in argon shock wave structure. Nakagawa and Wisler[65] measured the electron temperature in hydrogen shock waves and compared excited electronic state populations with predictions. They found that the higher excited states tended to equilibrate with the electrons at the electron temperature much faster than the lower excited states.

Leibowitz[1,9] studied ionization rates behind shock waves in hydrogen-helium mixtures by measuring hydrogen line and continuum radiation. He developed a reaction scheme which included dissociation and a two-step excitation-ionization mechanism for hydrogen ionization by atom-atom and electron-atom collisions. He achieved good agreement between the numerical predictions and the experimental measurements. The excited states of hydrogen were assumed to be in equilibrium with the electrons at the electron temperature. The electron temperature was found to be significantly lower than the atom temperature throughout most of the relaxation region.

Shock Wave Precursors

The presence of electrons in front of hypersonic shocks has been observed [66-80] and theoretically investigated by several persons [81-102]. These precursors are important in atmospheric entry because they influence the propagation of electromagnetic radiation in the vicinity of the entry body. This affects identification of and/or communication with the vehicle. The precursor must be accounted for in interpreting the data a scientific probe gathers on atmospheric entry. Considerable effort has been spent determining the influence of the precursor on heat transfer to atmospheric entry vehicles [1-4,103].

Precursor effects must be accounted for in the study of shock wave structure, since the precursor region is coupled to the relaxation region by the radiative transfer. The coupling of the precursor to the relaxation region has been studied by several people [8,41,45,46,54,55,104,105]. In addition, astrophysicists must understand precursors because they occur in the shock structure of variable stars [106], interstellar gas [107], and certain solar events [108].

Precursors in Atomic Gases

Throughout the literature controversy exists as to whether the precursor ionization observed in shock tubes is produced by electron diffusion from the

high pressure region behind the shock, or photoionization from the ultraviolet radiation emitted in the region behind the shock. Photoemission from the shock tube walls has also been considered as a possible source of the precursor. Many experiments have been undertaken to determine the mechanism for electron production. The earlier work leaned toward electron diffusion and photoemission[66-69]; however, more recent experiments have conclusively shown that photoionization of the gas ahead of the shock is the main mechanism for producing precursors[72-76].

Precursor photoionization may occur either as a one-step process wherein the electron is freed from the ground state of the cold gas in front of the shock by the absorption of ground state continuum radiation, or as a two-step process wherein the atom is first excited by line radiation and then ionized by excited state continuum radiation. These processes are shown schematically in Fig. A-2. Lagar'Kov and Yakubov[85], Murty[91], Vulliet[92], Dobbins[96] and Nelson[102] have investigated the importance of line radiation in the precursor and the coupling of line radiation and excited state continuum radiation in the precursor. Precursors caused by photoionization gaseous impurities have been investigated for trace amounts of hydrogen impurity in argon shock waves[74, 90]. The electron temperature in the precursor has been measured[30].

The earliest precursor experiments were performed by Hollyer[66] in a metal pressure driven shock tube. He investigated Mach 9 shocks in argon at pressures less than one mm Hg, using Langmuir probes. Far ahead of the shock his probes collected only electrons. Thus, he concluded that photoemission from the shock tube wall, due to radiation emitted from the shocked gas, was responsible for the precursor.

Gloersen[69] experimented with xenon in a pressure driven pyrex shock tube at pressures from 0.75 to 4.0 mm Hg using probes wrapped around the outside of the tube. He observed two precursors, one traveling at about the speed of light

and one at the speed of the shock front. The fast precursor was attributed to photoemission from the shock tube walls, while the slow precursor was thought to be caused by collisional ionization, or photoionization of impurities at the shock front. Weymann, et. al.[67,77,78] used electrostatic and magnetic probes in a shock tube setup similar to that of Gloersen to investigate argon shock waves at Mach numbers from 8 to 12 and pressures from 2.5 to 10 mm Hg. They first concluded that the precursor was caused by diffusion of electrons from behind the shock wave because the electrostatic probe signals were negative and the magnetic probes indicated that electrons were moving ahead of the shock. They reasoned that the large concentration gradients just behind the shock and high thermal velocities of the electrons were responsible for the electron diffusion. However, a later set of experiments at lower impurity levels showed that photoionization was the cause of the precursor. McRae and Leadon[79] also found impurities to be the main source of precursor ionization in their experiments in xenon.

Zivanovic[72] investigated precursors with a ballistic range in which small copper spheres were fired up to 6,600 meters per second into air at pressures from 1 to 30 mm Hg. Electron density measurements were made utilizing a biased electrode plate, shielded by a screen. The bias established an electric field between the screen and the electrode plate. The field forced all the electrons which were photoemitted from the plate to return to the plate. Hence, only the electrons produced from diffusion and photoionization contributed to the current through the plate, which was measured and related to the electron density. For a series of experiments a second grid was placed in front of the screen and biased so that it would repel all the diffusion electrons. Thus, these experiments measured only the electrons generated by photoionization between the grid and the screen. The measured current was the same in the experiments which measured only photoionization electrons and those which measured both diffusion and

photoionization electrons. Thus, it was concluded that the precursor was caused mainly by photoionization.

Lederman and Wilson[76] measured argon precursor electron densities with a microwave resonant cavity and an electrostatic probe. The Mach numbers varied between 10.5 and 13.5 and the argon pressures were between 0.76 and 15 mm Hg. Some of the experiments were performed with a "venetian blind" in the shock tube. The "venetian blind" allowed electrons to diffuse through it and blocked the radiation. Their results agreed with those of Zivanovic in that photoionization, rather than electron diffusion, was the major cause of the precursor ionization.

Precursors in Diatomic Gases

The literature involving the influence of precursors in diatomic gases is usually involved in an engineering application. In most cases it involves the effect of the precursor on blunt body heating for planetary entry conditions.

Precursors in diatomic gases have been observed[63,75] and theoretically modeled[93,94,99,103]. Much of the radiation energy emitted in the shock layer relaxation region is lost; however, when the photon energy is greater than the molecular dissociation energy, it is strongly absorbed in the precursor region. This absorbed energy dissociates and ionizes the gas. It also increases the gas temperature and pressure. The change in the free stream flow properties may change the flow characteristics of the shock layer and the heat transfer to the body.

Mermagen[75] observed precursors in front of Lexan cylinders, launched from a light gas gun at velocities from 3900 to 5500 m/sec into air at a pressure of 50 mm. Hg. The excited and ionized gases in shock layer around the model emitted infrared radiation which pre-excited the cold gas in front of the shock. The shock layer was populated by excited and ionized air, including contaminants, as well as ablation products from the Lexan. Lin[63] presented evidence of a

"photoionization halo" surrounding the first manned Mercury orbital flight during its re-entry.

Radiative preheating of the cold gas by absorption of photons emitted from the hot shock layer was considered in most shock tube studies of shock wave structure by the late 1960's; however, it was usually neglected in the analysis of the blunt body shock layer problem. Yoshikawa[109] considered the precursor influence on the blunt body shock layer for a gray gas and a linear relationship between the Planck emissive power and the gas enthalpy. Lasher and Wilson[103] considered an uncoupled precursor, in which they used available blunt body shock layer solutions to obtain a first approximation of the radiative energy available to form the precursor. The precursor effects then preturbed the free stream conditions and changed the shock layer solutions. Thus, their solutions were valid when the precursor effects were small. Lasher and Wilson included the spectral variation of the radiation and radiation properties. Liu[97] investigated precursor effects on the heating of vehicles entering the earth's atmosphere in terms of the ratio of radiative to convective flux. The precursor influence was negligible when the radiative to convective flux ratio was less than unity.

Smith[93] and Edwards[94] calculated electron densities in the precursor of a shock preceding a blunt body for earth atmospheric entry. Smith used a simple microscopic model for air and included three-dimensional effects by modeling the body and shock layer as a point source. He calculated velocity, pressure, density and electron concentrations in the precursor region. Edwards used a more descriptive microscopic model for air and modeled the blunt body shock layer as a constant temperature disk. A constant fraction of the radiation absorbed in the precursor was assumed to yield the electron concentration along the stagnation streamline. The influence of the precursor on the blunt body heating for lunar returns was predicted to be negligible.

In the past 10 years there has been considerable interest in designing probes to enter the atmospheres of the outer planets, like Jupiter and Saturn. These atmospheres are thought to be composed of mainly hydrogen and helium. Thus, considerable effort has been put forth to investigate the heating of vehicles entering hydrogen-helium atmospheres. As a part of this effort Tiwari and Szema[3-4] have investigated the effect of precursors on the heating of vehicles traveling in hydrogen-helium atmospheres. They solved the radiation coupled precursor-shock layer problem taking into account many details such as viscous flow, spectral details of the radiative transfer, thermal non-equilibrium in the shock layer, multi-dimensional flow fields, finite chemical rates, etc. Their results generally show that the precursor effects should increase the heat transfer to the entry vehicle.

APPENDIX B: FORMULATION OF RADIATIVE INTENSITY

This section of the Appendix contains a general formulation of radiation intensity. The medium through which the incident radiation field passes is assumed to be an atomic plasma. The plasma is assumed to consist of ground and excited state atoms, ions, and electrons. In formulating the radiation intensity, spontaneous and induced emission and absorption will be considered. This model makes it possible to study the coupling of line radiation (bound-bound processes) with continuum radiation (bound-free processes).

The fundamental quantities of atomic radiation are the Einstein coefficients[110]. The Einstein coefficient, $A_{u\ell}$, for spontaneous emission is defined such that the probability per unit time for a spontaneous transition from upper state u to lower state ℓ with the emission of radiation in the solid angle $d\Omega$ is

$$A_{u\ell} \, d\Omega, \quad (1/\text{sec}) \tag{1}$$

The total number of spontaneous transitions from state u to ℓ per unit volume per unit time with the emission of radiation in $d\Omega$ is

$$n_a(u) \, A_{u\ell} \, d\Omega, \quad (1/(\text{cm}^3\text{-sec})) \tag{2}$$

where $n_a(u)$ is the number density of the upper excited state. The energy emitted per transition is equal to $h\nu_{u\ell}$ when the influence of the surrounding plasma is negligible; however, in real situations the transition can occur with the emission of almost any amount of energy. A certain value of emitted energy is determined by the emission line shape, ψ_ν, (sec) which essentially represents the influence of the neighboring gas on the atom of interest. The total radiation intensity emitted in the frequency interval ν to $\nu + d\nu$ per unit time is

$$h\nu \, n_a(u) \, A_{u\ell} \, \psi_\nu \, d\Omega d\nu \quad (\text{ergs}/(\text{cm}^3\text{-sec})). \tag{3}$$

Spontaneous emission also occurs when a free electron recombines to a bound state. In the model, there are several possible free-bound transitions: free to first excited (f to 2) and free to ground (f to 1), etc.

The probability that an electron-ion encounter occurs with the free electron losing energy, $h\nu = \chi_\ell + \eta$, by emitting radiation within the solid angle $d\Omega$ is $A_{f\ell}\, d\Omega$. After the encounter, the electron-ion pair becomes an atom with the electron in state ℓ. For the model, ℓ can be any bound electronic level.

Spontaneous emission cannot occur unless an electron and ion undergo an encounter. The number of collisions between electrons with energy in the range η, $\eta + d\eta$ and ions per unit time per unit volume, is

$$A_{f\ell}\ n_e n_i\ f_e(\eta)\ d\eta d\Omega \quad 1/(\text{cm}^3\text{-sec}) \tag{4}$$

where $f_e(\eta)$ is the energy distribution function for the electrons. For a Maxwellian distribution at the electron temperature T_e,

$$f(\eta)d\eta = 2\pi(\pi k T_e)^{-3/2}(\eta)^{1/2}\exp(-\eta/kT_e)d\eta. \tag{5}$$

The probability of a spontaneous emission, with the creation of an atom, is equal to the probability of an emission times the number of electron-ion collisions. The total radiation intensity emitted in the frequency interval ν to $\nu + d\nu$ per unit volume per unit time in the solid angle $d\Omega$ by all electron-ion spontaneous emissions is

$$h\nu\ A_{f\ell}\ n_e n_i\ f_e(\eta)\ d\eta d\Omega, \quad (\text{ergs}/(\text{cm}^3\text{-sec})) \tag{6}$$

where $d\eta = hd\nu$. This process emits continuum radiation; whereas, the process of Eq. (3) emits line radiation.

The Einstein coefficient for absorption $B_{\ell u}$ is defined such that in a radiation field of specific intensity, I_ν, the probability per unit time for a transition from state ℓ to u with the absorption of radiant energy in the

frequency range ν to $\nu + d\nu$ in the solid angle $d\Omega$ is

$$B_{\ell u} \; \phi_\nu \; I_\nu \; d\nu d\Omega, \quad (1/\text{sec}) \tag{7}$$

where ϕ_ν is the absorption line shape. The total number of transitions from state ℓ to u per unit volume per unit time as a result of the absorption of radiation is

$$n_a(\ell) \; B_{\ell u} \; \phi_\nu \; I_\nu \; d\Omega d\nu, \quad (1/\text{cm}^3\text{-sec})) \tag{8}$$

The total amount of radiation absorbed from the radiation field in the frequency interval ν to $\nu + d\nu$ per unit volume per unit time in the solid angle $d\Omega$ is

$$h\nu \; n_a(\ell) \; B_{\ell u} \; \phi_\nu \; I_\nu \; d\Omega d\nu, \quad (\text{ergs}/(\text{cm}^3\text{-sec})) \tag{9}$$

This process represents a bound-bound process. The line shape, ϕ_ν, is used because the probability of the absorption of energy is related to the magnitude of the energy, through the line shape.

The bound-free process must also be considered. Equation (9) can be used to represent the bound-free process if the subscript u is changed to f. The continuum absorption can then be written as

$$h\nu \; n_a(\ell) \; B_{\ell f} \; I_\nu \; d\Omega d\nu. \quad (\text{ergs}/(\text{cm}^3\text{-sec})) \tag{10}$$

where ℓ represents any bound electronic state.

Emission of radiation may also be induced by the radiation field. The Einstein coefficient for induced emission is defined such that in a radiation field of specific intensity, I_ν, the probability per unit time for a transition from state u to ℓ as a result of induced emission in the frequency range ν to $\nu + d\nu$ and in the solid angle $d\Omega$ is

$$B_{u\ell} \; I_\nu \; d\Omega d\nu. \tag{11}$$

The total number of transitions from state u to ℓ per unit volume per unit time as a result of induced emission is

$$n_a(u) \, B_{u\ell} \, I_\nu \, d\Omega, \quad (1/cm^3\text{-sec}))$$

(12)

The total amount of radiation emitted in the frequency interval ν to $\nu + d\nu$ in the solid angle $d\Omega$ per unit volume per unit time by induced emission is then

$$h\nu \, n_a(u) \, B_{u\ell} \, \psi_\nu \, I_\nu \, d\Omega d\nu, \quad (ergs/(cm^3\text{-sec}))$$

(13)

where again the line shape, ψ_ν, is introduced because it is the probability density function of the magnitude of the emitted energy.

Equation (13) represents bound-bound induced emission. The induced emission which results in continuum radiation must also be considered. Induced emission, when the initial states are free states, depends upon the number of collisions between the electrons and ions. Using Eq. (4) and Eq. (13), one can write an expression for the continuum induced emission. The radiation emitted in the frequency interval, ν to $\nu + d\nu$, in the solid angle $d\Omega$ per unit volume per unit time by free-bound induced emission is

$$h\nu \, B_{f\ell} \, n_e n_i \, f_e(\eta) \, I_\nu \, d\eta d\Omega, \quad (ergs/(cm^3\text{-sec}))$$

(14)

where $d\eta = hd\nu$. During the process, the electron loses energy, $h\nu = \chi_\ell + \eta$, while the ion gains energy, χ_ℓ; the recombination is at the ℓth level of the atom, as the electron-ion pair create an atom in state ℓ.

The rate of change of the radiation intensity at a point within the solid angle, $d\Omega$, in the frequency range, ν to $\nu + d\nu$, in the direction s is the sum of the contributions (both negative and positive) given by Eqs. (3), (6), (9), (10), (13), and (14):

$$\frac{dI_\nu}{ds} \, d\nu d\Omega = \{-[n_a(\ell) \, B_{\ell f} + n_a(\ell) \, B_{\ell u} \, \phi_\nu - n_e n_1 \, B_{f\ell} \, f_e(\eta)$$

$$- n_a(u) \, B_{u\ell} \, \psi_\nu] \, h\nu I_\nu + [n_a(u) \, A_{u\ell} \, \psi_\nu \qquad (15)$$

$$+ n_e n_1 \, A_{f\ell} \, f_e(\eta)] \, h\nu\} \, d\nu d\Omega.$$

The processes represented on the right-hand of Eq. (15) in the term multiplied by I_ν are respectively continuum absorption, Eq. (10), line absorption, Eq. (9), continuum induced emission, Eq. (14), and line induced emission, Eq. (13). The second term, which is multiplied by $h\nu$ represents line spontaneous emission, from Eq. (3) and continuum spontaneous emission, from Eq. (6), respectively.

Equation (15) represents the general form of the radiation transfer equation. It can be rewritten as

$$\frac{dI_\nu}{ds} = -\{n_a(\ell) \, B_{\ell f} [1 - \frac{n_e n_1}{n_a(\ell)} \, f_e(\eta) \, \frac{B_{f\ell}}{B_{\ell f}}]$$

$$+ n_a(\ell) \, B_{\ell u} \, \phi_\nu \, [1 - \frac{n_a(u)}{n_a(\ell)} \, \frac{B_{u\ell}}{B_{\ell u}} \, \frac{\psi_\nu}{\phi_\nu}]\} \, h\nu I_\nu \qquad (16)$$

$$+ n_a(\ell) \, B_{\ell u} \, \phi_\nu \, \frac{n_a(u) A_{u\ell}}{n_a(\ell) B_{\ell u}} \, \frac{\psi_\nu}{\phi_\nu} \, h\nu + n_\ell \, B_{\ell f} \, \frac{n_e n_1}{n_a(\ell)} \, f_e(\eta) \, \frac{A_{f\ell}}{B_{\ell f}} \, h\nu.$$

$$\ell = 1,2,\ldots L-1$$

$$u = 2,3,\ldots L$$

where L is the total number of bound electronic states. In what follows the absorption and emission line slopes will be taken as the same, $\psi_\nu = \phi_\nu$.

The relationships between the Einstein coefficients can be found by considering the equilibrium case. If the gas is in equilibrium, $\frac{dI_\nu}{ds} = 0$ and I_ν is given by the Planck function

$$B_\nu = \frac{2h\nu^3}{c^2} \frac{1}{\exp(\frac{h\nu}{kT}) - 1} \qquad (17)$$

Considering only the line transitions, those terms involving ϕ_ν in Eq. (16), one can write at equilibrium

$$I_\nu = \frac{n_a(u)A_{u\ell}}{n_a(\ell)B_{\ell u}} \frac{1}{1 - \dfrac{n_a(u)B_{u\ell}}{n_a(\ell)B_{\ell u}}} \tag{18}$$

However, at equilibrium

$$\frac{n_a^*(u)}{n_a^*(\ell)} = \frac{g_u}{g_\ell} \exp(-\chi_{u\ell}/kT_a) \tag{19}$$

where g_ℓ and g_u are the degeneracies of the states ℓ and u respectively, T_a is the atom temperature, and $\chi_{\ell u}$ is the energy difference between the states. To force Eq. (18) to agree with the Planck function one must have

$$\frac{A_{u\ell}}{B_{\ell u}} = \frac{g_\ell}{g_u} \frac{2h\nu^3}{c^2} \quad \text{and} \quad \frac{B_{u\ell}}{B_{\ell u}} = \frac{g_\ell}{g_u} \tag{20a}$$

or that

$$\frac{A_{u\ell}}{B_{\ell u}} = \frac{2h\nu^3}{c^2} \left[\frac{n_a^*(\ell)}{n_a^*(u)}\right]_{T_a} \exp\left(-\frac{h\nu_{\ell u}}{kT_a}\right) \qquad \frac{B_{u\ell}}{B_{\ell u}} = \left[\frac{n_a^*(\ell)}{n_a^*(u)}\right]_{T_a} \exp\left(-\frac{h\nu_{\ell u}}{kT_a}\right) \tag{20b}$$

Then one can write I_ν as

$$I_\nu = \frac{2h\nu^3}{c^2} \frac{[n_a(u)/n_a(\ell)] \, [n_a^*(\ell)/n_a^*(u)]_{T_a} \exp(-h\nu_{\ell u}/kT_a)}{1 - [n_a(u)/n_a(\ell)] \, [n_a^*(\ell)/n_a^*(u)]_{T_a} \exp(-h\nu_{\ell u}/kT_a)} \tag{20c}$$

which approaches the Planck function as the gas goes to equilibrium. This then defines the three Einstein coefficients, if one of them is known.

When the continuum portion of the intensity is considered, one must define the Einstein coefficients as

$$A_{f\ell}/B_{\ell f} = 2h\nu^3/c^2 \qquad B_{f\ell}/B_{\ell f} = g_\ell/(g_f g_i) \tag{21}$$

where g_f is the degeneracy of the free election states with energies between η and $\eta + d\eta$;[111]

$$g_f = \frac{2(4\pi)(m_e)^{3/2}}{h^3} (2\eta)^{1/2} \, d\eta. \tag{22}$$

The factor g_ℓ is the degeneracy of the ℓth bound state, and g_i is the degeneracy of the ion. The ion is normally in its ground state. In Eq. (22), g_f has units of $1/cm^3$, so that it represents the degeneracy per unit volume. One must consider the relation $\dfrac{n_e n_i}{n_a(\ell)} f_e(\eta) \dfrac{B_{f\ell}}{B_{\ell f}}$ where

$$f_e(\eta) \, d\eta = \frac{2\pi}{(\pi k T_e)^{3/2}} (\eta)^{1/2} \exp(-\eta/kT_e) \, d\eta \tag{23}$$

represents the fraction of electrons with energies between η and $\eta + d\eta$, where $\eta = \chi_{\ell u} + h\nu$. The relation can be written as

$$\frac{n_e n_i}{n_a(\ell)} \frac{g_\ell \, h^3 \, \exp(-\eta/kT_\nu)}{2 g_i \, (2\pi m_e kT_e)^{3/2}}$$

using Eqs. (21), (22), and (23). At equilibrium the ratio of the population of the electrons and ions to that of bound state ℓ is given by Saha equation[4]

$$\left[\frac{n_i^\ast n_e^\ast}{n_e^\ast(\ell)}\right]_{T_e} = 2 \frac{g_i}{g_\ell} \frac{(2\pi m_e kT_e)^{3/2} \exp(-\chi_\ell/kT_e)}{h^3} \tag{24}$$

Thus, the relation can be written as

$$\frac{n_e n_i}{n_a(\ell)} \left[\frac{n_a^\ast(\ell)}{n_i^\ast n_e^\ast}\right]_{T_e} \exp(-h\nu/kT_e) \tag{25}$$

where the definition of η was used ($\eta = \chi_\ell + h\nu$). Using Eq. (25), one can write the continuum intensity as

$$I_\nu = \frac{\dfrac{n_e n_i}{n_a(\ell)} \left[\dfrac{n_a(\ell)}{n_e n_i}\right]_{T_e} \exp(-h\nu/kT_e) \, A_{f\ell}/B_{\ell f}}{1 - \dfrac{n_e n_i}{n_a(\ell)} \left[\dfrac{n_a^\ast(\ell)}{n_e^\ast n_i^\ast}\right]_{T_e} \exp(-h\nu/kT_e)} \tag{26}$$

Now as the gas goes to equilibrium and using equation (21) for $A_{f\ell}/B_{\ell f}$, $I_\nu \to B_\nu$, the Planck function. Note that Eq. (26) is a function of the electron

temperature T_e.

Using the definitions given by Eqs. (20), (21), and (25), one can rewrite Eq. (16) as

$$\frac{dI_\nu}{ds} = - \{n_a(\ell)B_{\ell f}[1 - Z_{\ell f}\exp(-h\nu/kT_e)] + n_a(\ell)B_{\ell u}\phi_\nu$$

$$\cdot [1 - Z_{\ell u}\exp(-h\nu/kT)]\}h\nu I_\nu \qquad (27)$$

$$+ \{n_a(\ell)B_{\ell f}Z_{\ell f}\exp(-h\nu/kT_e)h\nu + n_a(\ell)B_{\ell u}\phi_\nu Z_{\ell u}\exp(-h\nu/kT)h\nu\}\frac{2h\nu^3}{c^2}$$

where

$$Z_{\ell f} = \frac{n_e n_i}{n_a(\ell)}\left[\frac{n_a^*(\ell)}{n_e^* n_i^*}\right]_{T_e} \qquad (28)$$

and

$$Z_{\ell u} = \frac{n_a(u)}{n_a(\ell)}\left[\frac{n_a^*(\ell)}{n_a^*(u)}\right]_{T_a} \qquad (29)$$

and ℓ is summed over all bound levels $\ell = 1, 2 \ldots L$ and u is summed over levels $\ell + 1, \ell + 2, \ldots L$. If the gas is in equilibrium, $Z_{\ell f}$ and $Z_{\ell u}$ go to unity and dI_ν/ds goes to zero. The general form of the equation of radiative transfer is[110]

$$\frac{dI_\nu}{ds} = - k_\nu I_\nu + \epsilon_\nu \qquad (30)$$

where k_ν is the absorption coefficient, and ϵ_ν is the emission function. From Eq. (27), one sees that

$$k_\nu = \{n_a(\ell)B_{\ell f}[1 - Z_{\ell f}\exp(-h\nu/kT_e)]$$

$$+ n_a(\ell)B_{\ell u}\phi_\nu[1 - Z_{\ell u}\exp(-h\nu/kT)]\}h\nu \qquad (31)$$

and

$$\epsilon_\nu = \frac{2h\nu^3}{c^2}[n_a(\ell)B_{\ell f}Z_{\ell f}\exp(-h\nu/kT_e) + n_a(\ell)B_{\ell u}\phi_\nu Z_{\ell u}\exp(-h\nu/kT]h\nu \qquad (32)$$

In the limit of equilibrium, k_ν and ϵ_ν for the lines agree with relations given by Jefferies[112] when the absorption and emission profiles are the same. The radiation transfer equation is simplified by converting the independent variable from s to τ_ν, the optical depth.

$$\tau_\nu = \int k_\nu dy \tag{33}$$

The equation of transfer can then be written as

$$\mu \frac{dI_\nu}{d\tau_\nu} = I_\nu - S_\nu \tag{34}$$

where $S_\nu = \epsilon_\nu / k_\nu$ and is known as the source function, and $y = \mu s$, where μ is the cosine of the angle between the general direction of radiation intensity propagation s and the coordinate y. The source function becomes

$$S_\nu = \frac{2h\nu^3}{c^2} \frac{n_a(\ell)B_{\ell f}Z_{\ell f}e^{-\frac{h\nu}{kT_e}} + n_a(\ell)B_{\ell u}\phi_\nu Z_{\ell u}e^{-\frac{h\nu}{kT}}}{n_a(\ell)B_{\ell f}(1 - Z_{\ell f}e^{-\frac{h\nu}{kT_e}}) + n_a(\ell)B_{\ell u}\phi_\nu(1 - Z_{\ell u}e^{-\frac{h\nu}{kT}})} \tag{35}$$

The radiative transfer can now be evaluated, if the line shape, ϕ_ν, is known and the Einstein coefficients, $B_{\ell f}$ and $B_{\ell u}$, can be determined. $B_{\ell f}$ and $B_{\ell u}$ are functions of the particular gas of interest. Note that in the limit of equilibrium, S_ν reduces to the Planck function. Note also that the units of $B_{\ell f}$ are cm^2/erg and that the units of $B_{\ell u}$ are $cm^2/(erg\text{-}sec)$ because $B_{\ell u}\phi_\nu$ must have units of cm^2/erg.

The absorption coefficient can be written in terms of the cross sections as

$$k_\nu = n_a(\ell)\sigma_{\ell f}(1 - Z_{\ell f}e^{-\frac{h\nu}{kT_e}}) + n_a(\ell)\sigma_{\ell u}(1 - Z_{\ell u}e^{-\frac{h\nu}{kT}}) \tag{36}$$

where the cross sections are defined as

$$\sigma_{\ell f} = h\nu B_{\ell f} \quad (cm^2) \tag{37}$$

and

$$\sigma_{\ell u} = h\nu\phi_\nu B_{\ell u} \quad (cm^2) \tag{38}$$

In terms of the cross sections, the source function becomes

$$S_\nu = \frac{2h\nu^3}{c^2} \; \frac{n_a(\ell)\sigma_{\ell f}Z_{\ell f}e^{-\frac{h\nu}{kT_e}} + n_a(\ell)\sigma_{\ell u}Z_{\ell u}e^{-\frac{h\nu}{kT}}}{n_a(\ell)\sigma_{\ell f}(1 - Z_{\ell f}e^{-\frac{h\nu}{kT_e}}) + n_a(\ell)\sigma_{\ell u}(1 - Z_{\ell u}e^{-\frac{h\nu}{kT}})} \tag{39}$$

The cross sections are functions of the gas and the various transitions. The general solution of the equation of transfer for the geometry shown in Fig. B-1 is[110]

$$I_\nu(\tau_\nu,\mu) = \begin{cases} I_\nu^1(\tau_\nu^1,\mu)e^{(\tau_\nu^1-\tau_\nu)/\mu} - \displaystyle\int_{\tau_\nu}^{\tau_\nu^1} S_\nu(t_\nu)e^{(t_\nu-\tau_\nu)/\mu}\frac{dt_\nu}{\mu} & (u<0) \\[20pt] I_\nu^0(0,\mu)e^{-\tau_\nu/\mu} + \displaystyle\int_0^{\tau_\nu} S_\nu(t_\nu)e^{-(\tau_\nu-t_\nu)/\mu}\frac{dt_\nu}{\mu} & (u\geq 0) \end{cases} \tag{40}$$

where $I_\nu^1(\tau_\nu^1,\mu)$ is the intensity incident on the boundary at τ_ν^1, and I_ν^0 $(0,\mu)$ is the incident intensity on the boundary at zero. The contribution to the radiative flux in the frequency range ν to $\nu + d\nu$ is
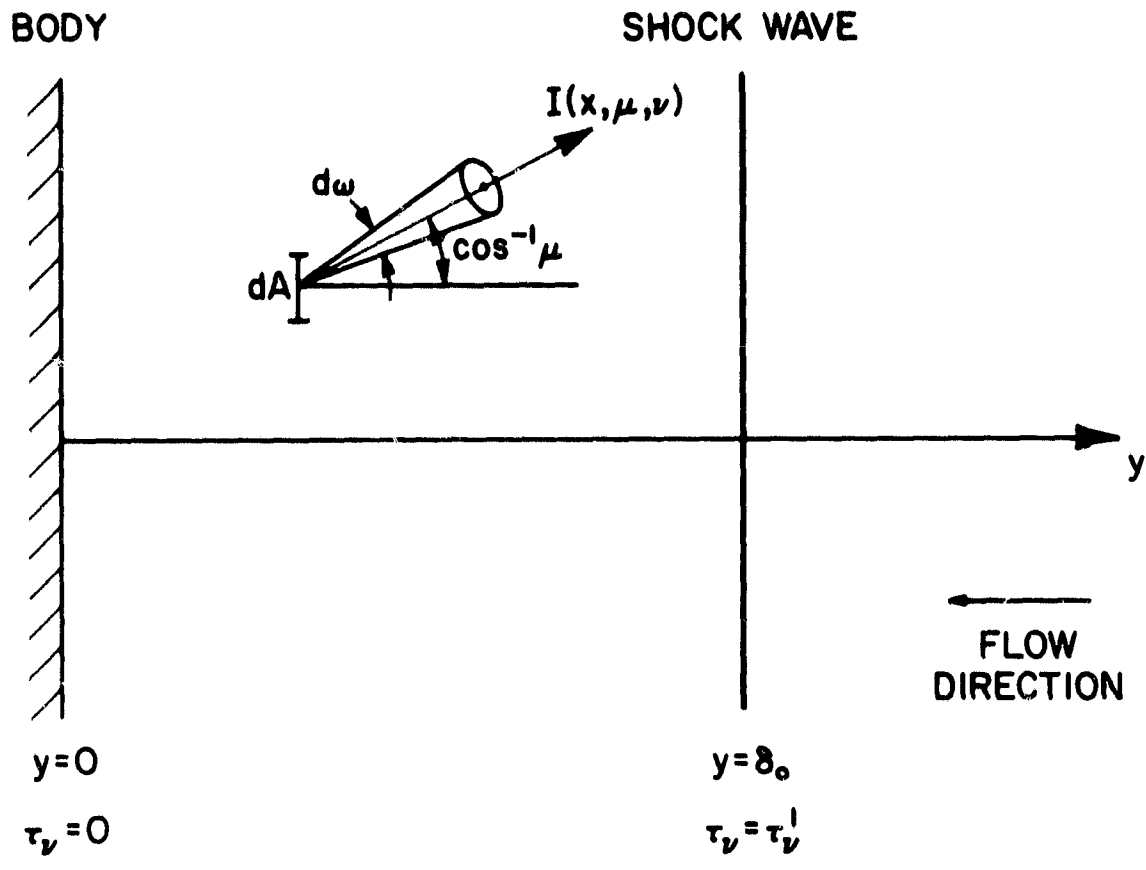
$$q_R(\tau_\nu,\nu) = 2\pi\int_{-1}^{1} \mu I_\nu(\tau_\nu,\mu) \, d\mu. \tag{41}$$

Figure B-1. Radiation Geometry.